

Spatial Clustering of High Redshift Lyman Break Galaxies

Charles Jose^{1*}, Kandaswamy Subramanian^{1†}, Raghunathan Srianand^{1‡} and Saumyadip Samui^{2§}

¹*IUCAA, Post Bag 4, Pune University Campus, Ganeshkhind, Pune 411007, India*

²*Astrophysics and Cosmology Research Unit, School of Physics, UKZN, Durban 4001, South Africa*

25 October 2018

ABSTRACT

We present a physically motivated semi-analytic model to understand the clustering of high redshift Lyman break galaxies (LBGs). We show that the model parameters constrained by the observed luminosity function, can be used to predict large scale (i.e. $\theta \geq 80''$) bias and angular correlation function of galaxies. These predictions are shown to reproduce the observations remarkably well. We then adopt these model parameters to calculate the halo occupation distribution (HOD) using the conditional mass function. The halo model using this HOD is shown to provide a reasonably good fit to the observed clustering of LBGs at both large and small ($\theta < 10''$) angular scales for the whole range of $z = 3 - 5$ and limiting magnitudes. However, our models underpredict the clustering amplitude at intermediate angular scales, where quasi-linear effects are important. The average mass of halos contributing to the observed clustering is found to be $6.2 \times 10^{11} M_{\odot}$ and the characteristic mass of a parent halo hosting satellite galaxies is $1.2 \times 10^{12} M_{\odot}$ for a limiting absolute magnitude of -20.5 at $z = 4$. For a given threshold luminosity these masses decrease with increasing z and at any given z these are found to increase with increasing value of threshold luminosity. Our physical model for the HOD suggests that approximately 40% of the halos above a minimum mass M_{min} , can host detectable central galaxies and about 5 – 10% of these halos are likely to also host a detectable satellite. These satellites form typically a dynamical timescale prior to the formation of the parent halo. The small angular scale clustering is mainly due to central-satellite pairs rather than few large clusters. It is quite sensitive to changes in the duration of star formation in a halo and hence could provide a probe of this quantity. The present data favor star formation in a halo lasting typically for a few dynamical time-scales, with 50% of stars formed in a time $T \sim 300 - 500$ Myr for dark matter halos that collapse in the redshift range of 5.5 – 3.5. Our models also reproduce different known trends between parameters related to star formation.

Key words: cosmology: theory – cosmology: large-scale structure of universe – galaxies: formation – galaxies: high-redshift – galaxies: luminosity function – galaxies: statistics – galaxy: haloes

1 INTRODUCTION

Over the past decade there has been a growing wealth of observations probing the properties of high redshift galaxies. Various surveys, using the Lyman break color selection technique (Madau et al. 1996; Steidel et al. 1996; Adelberger et al. 1998; Steidel et al. 1998), have detected a substantial number of high redshift galaxies, up to $z \sim 10$.

This has resulted in reasonably good estimates of luminosity functions (LF) of these Lyman break galaxies (LBG) up to $z \sim 8$ (Bouwens et al. 2007, 2008; Reddy et al. 2008; van der Burg et al. 2010) and also LBG clustering up to $z \sim 5$ (Giavalisco & Dickinson 2001; Porciani & Giavalisco 2002; Ouchi et al. 2004; Adelberger et al. 2005; Ouchi et al. 2005; Kashikawa et al. 2006; Lee et al. 2006; Hildebrandt et al. 2009; Savoy et al. 2011; Bielby et al. 2011). It is important to explain these observations and understand their implications for galaxy formation.

In the hierarchical model of structure formation galaxies form in virialized dark matter halos. These in turn result from the growth and gravitational collapse of initial Gaus-

* charles@iucaa.ernet.in

† kandu@iucaa.ernet.in

‡ anand@iucaa.ernet.in

§ samuis@ukzn.ac.za

sian density perturbations. Thus the statistical properties of galaxies are determined by the statistics of the parent halo population, given a model for how stars form inside these halos. The properties of dark matter halos are quite well understood using N-body simulations (Springel et al. 2005) and analytical models like the halo model of large scale structure (Cooray & Sheth 2002). These approaches provide the abundance, spatial distribution and merger history of dark matter halos. Numerical simulations also suggest a possible universal dark matter halo density profile, NFW profile (Navarro et al. 1997). Given the above inputs on dark matter halo properties and a specific model of galaxy formation inside these halos, it is possible to explain the two major observables of galaxies, their luminosity function and clustering. In addition, such models can throw light on the complex physics of galaxy formation, such as rate and duration of star formation, feedback mechanisms etc.

There has been extensive modelling of the luminosity functions and clustering of galaxies at low redshifts (Somerville & Primack 1999; Yang et al. 2003; Zheng et al. 2009; Zehavi et al. 2011). Several studies on understanding the LF of high redshift LBGs have also been carried out (Somerville et al. 2001; Benson et al. 2003; Stark et al. 2007; Khochfar et al. 2007). We have been exploring physically motivated semi-analytic models of galaxy formation to understand the LFs of LBGs and Lyman- α emitters, galactic winds and reionization of the intergalactic medium (Samui et al. 2007, 2008, 2009b,a, 2010). In our model, the luminosity of any galaxy is obtained from a physical model of star formation rate which depends on the mass and age of the hosting halo. We then combine this information with the formation rate of dark matter halos to obtain the LF of LBGs at various redshifts (see section 2 for details). These models have reproduced the LFs of high z LBGs from $z = 3 - 7$ reasonably well. In addition they constrain the efficiency of star formation and its duration in LBGs, and have also been used to set tight limits on the neutrino mass (Jose et al. 2011). We now wish to examine if our simple physical model for galaxy formation, combined with the halo model, can also explain the clustering of the high z LBGs.

Semi-analytical models of clustering involve giving a prescription for how many galaxies of different luminosities occupy a dark matter halo of a given mass. This is called the Halo occupation distribution (HOD) and is usually given in a parametrized form (Jing et al. 1998; Seljak 2000; Scoccimarro et al. 2001; Bullock et al. 2002a,b; Berlind & Weinberg 2002; van den Bosch et al. 2003; Berlind et al. 2003; Kravtsov et al. 2004; Zehavi et al. 2004; Hamana et al. 2004; Zehavi et al. 2005; Zheng et al. 2005; Hamana et al. 2006; Conroy et al. 2006; Lee et al. 2009). In our work we calculate the HOD without assuming any parametric form. Combining this with the dark matter halo abundance, bias and density profile, the galaxy clustering can be calculated.

To begin with we assume that each halo can host at most one visible central galaxy. By fitting the observed LF of LBGs, we find the masses of dark matter halos which host an LBG of a given luminosity. We then show that our prescription of star formation that fits the observed LF of LBGs can also simultaneously explain their large scale clustering ($\theta \geq 80''$). In order to also account for the small angular scale clustering we calculate how many subhalos hosting a

detectable satellite can form in a bigger parent halo using the conditional mass function (Cooray & Sheth 2002) and our star formation prescription. Thus we provide a method of calculating the HOD from first principles, which can then be used to predict the LBG clustering. Using our approach, we show that one can explain both the UV LFs and luminosity dependent clustering of LBGs and gain useful insights into galaxy formation.

The organization of this paper is as follows. In the next section we describe our physical model for computation of the LF of LBGs. In Section 3 we focus on the clustering of LBGs on large angular scales. We then turn to our physically motivated model to calculate the central and satellite contributions to the HOD and use these to obtain total angular correlation functions at all angular scales. Section 5 presents a comprehensive comparison of the total angular correlation function computed in various models with observations. A discussion of our results and conclusions are presented in the final section. For all calculations we adopt a flat Λ CDM universe with cosmological parameters consistent with 7 year Wilkinson Microwave Anisotropy Probe (WMAP7) observations (Larson et al. 2011). Accordingly we assume $\Omega_m = 0.27$, $\Omega_\Lambda = 0.73$, $\Omega_b = 0.045$, $h = 0.71$, $n_s = 0.963$ and $\sigma_8 = 0.801h^{-1}$ Mpc. Here Ω_i is the background density of any species 'i' in units of critical density ρ_c . The Hubble constant is $H_0 = 100h$ km s $^{-1}$ Mpc $^{-1}$

2 THE STAR FORMATION RATE AND LUMINOSITY FUNCTION

Our aim is to construct a self consistent semi-analytical model, that can explain the luminosity functions and clustering of high redshift LBGs. In this section, we briefly recall the semi analytical treatment of Samui et al. (2007) (hereafter SSS07) to model luminosity functions of high redshift LBGs [See also Samui et al. (2009b) (hereafter SSS09); Jose et al. (2011)] before presenting our prescription to calculate angular correlation functions at large and small scales. In this section we also show the relationship between star formation rate and stellar mass and stellar mass function predicted by our model.

In the models of SSS07, the star formation rate (\dot{M}_{SF}) in a dark matter halo of mass M collapsed at redshift z_c and observed at redshift z is given by (see, Chiu & Ostriker 2000; Choudhury & Srianand 2002),

$$\begin{aligned} \dot{M}_{SF}(M, z, z_c) &= f_* \left(\frac{\Omega_b}{\Omega_m} M \right) \frac{t(z) - t(z_c)}{\kappa^2 t_{dyn}^2(z_c)} \\ &\times \exp \left[-\frac{t(z) - t(z_c)}{\kappa t_{dyn}(z_c)} \right], \end{aligned} \quad (1)$$

where, f_* is the fraction of the total baryonic mass that is converted into stars over the entire lifetime of the galaxy and $t(z)$ is the age of the universe at redshift z ; thus $T(z, z_c) = t(z) - t(z_c)$ is the age of the galaxy at z . Further, $t_{dyn}(z_c)$ is the dynamical time scale of a halo collapsing at z_c and is given by

$$t_{dyn}(z_c) = \sqrt{\frac{3\pi}{32G\rho_{vir}(z_c)}}, \quad (2)$$

where $\rho_{vir}(z_c) = \Delta_c(z_c)\rho_c(z_c)$ with $\Delta_c(z_c)$ being the over

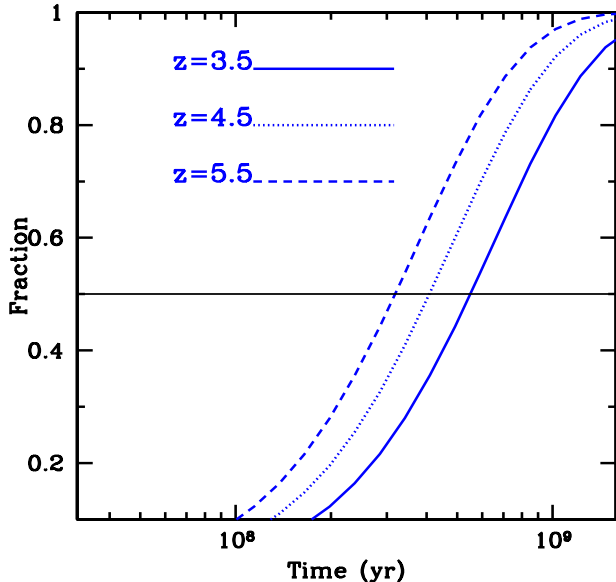


Figure 1. The fraction of stars formed in a halo in our model as a function of the age of the halo. The three different curves corresponds to halos formed at $z = 3.5, 4.5$ and 5.5 , assuming $\kappa = 1$.

density of the halo at the redshift of collapse, relative to the critical density $\rho_c(z_c) = [3H^2(z_c)/8\pi G]$. Typically t_{dyn} at any redshift is about 10% of the Hubble time at that redshift. Finally, κ in Eq. 1, is a parameter which governs the duration of the star formation activity. The star formation rate in a halo reaches a peak value when it's age is κt_{dyn} . Also over the life time of the galaxy a total baryon mass of $f_* M(\Omega_b/\Omega_m)$ will be converted into stars in any halo of mass M . In Fig. 1, we show the fraction of the stars formed inside a halo (i.e $M_*/[f_* M(\Omega_b/\Omega_m)]$) as a function of the age of the halo (here M_* is the stellar mass in the halo). From the figure one can see that 50 % of the stars are already in place within a time-scale of $T \sim 300 - 500$ Myr inside dark matter halos that collapses in the redshift range of $5.5 - 3.5$ for $\kappa = 1$. While the star formation can last for few 10^9 yrs, the period over which the galaxy is detectable depends on the halo mass and the luminosity threshold of the observations.

The stars are formed with a Salpeter IMF in the mass range $1 - 100 M_\odot$. The population synthesis code STARBURST99 (Leitherer et al. 1999) is used to obtain the rest frame luminosity (l_{1500}) at 1500 \AA as a function of time of a galaxy undergoing a burst of star formation. The assumed star formation rate of a galaxy, as given in Eq. (1), is then convolved with this burst luminosity to get the time evolution of the luminosity, L_{1500} , of an individual star forming galaxy (See Eq. (6) and Figure 1 of SSS07)

$$L_{1500}(T) = \int_T^0 \dot{M}_{SF}(T - \tau) l_{1500}(\tau) d\tau. \quad (3)$$

Due to dust absorption, only a fraction ($1/\eta$) of L_{1500} produced by the stars manages to escape the galaxy. This luminosity ($L = L_{1500}/\eta$) is then converted to a standard absolute AB magnitude M_{AB} , using the equation given by (Oke & Gunn 1983), to enable direct comparison with

the observed data. Having obtained the M_{AB} of individual galaxies we can compute the luminosity function $\Phi(M_{AB}, z)$ at any redshift z using,

$$\Phi(M_{AB}, z) dM_{AB} = \int_z^\infty dz_c \frac{dn(M(M_{AB}), z_c)}{dz_c} \frac{dM}{dL_{1500}} \quad (4)$$

$$\times \frac{dL_{1500}}{dM_{AB}} dM_{AB}.$$

Here $dn(M, z_c)/dz_c = \dot{n}(M, z_c) dt/dz_c$, and $\dot{n}(M, z_c) dM$ is the formation rate of halos in the mass range $(M, M+dM)$ at redshift z_c . SSS09 modelled this formation rate as the time derivative of Sheth & Tormen (1999) (hereafter ST) mass function as they are found to be good in reproducing the observed LF of high- z LBGs. Therefore we use $\dot{n}(M, z_c) = dn_{ST}(M, z_c)/dt$ where $n_{ST}(M, z_c)$ is the ST mass function at z_c . Also note that we use the notation $n(M)$ for dn/dM for convenience.

Star formation in a given halo also depends on the cooling efficiency of the gas and various other feedback processes. We assume that gas in halos with virial temperatures (T_{vir}) in excess of 10^4 K can cool (due to recombination line cooling from hydrogen and helium) and collapse to form stars. However the ionization of the IGM by UV photons increases the temperature of the gas thereby increasing the Jean's mass for collapse. Thus in ionized regions, we incorporate this feedback by a complete suppression of galaxy formation in halos with circular velocity $v_c \leq 35 \text{ km s}^{-1}$ and no suppression with $v_c \geq V_u = 95 \text{ km s}^{-1}$ (Bromm & Loeb 2002). For intermediate circular velocities, a linear fit from 1 to 0 is adopted as the suppression factor [Bromm & Loeb (2002); see also Benson et al. (2002); Dijkstra et al. (2004), SSS07]. SSS07 found that this feedback mechanism naturally leads to the observed flattening of the LF at the low luminosity end.

In our models, we also incorporate the possible Active Galactic Nuclei (AGN) feedback that suppresses star formation in the high mass halos, by multiplying the star formation rate by a factor $[1 + M/M_{agn}]^{-\beta}$. This decreases the star formation activity in high mass halos above a characteristic mass scale M_{agn} , which is believed to be $\sim 10^{12} M_\odot$ (see Bower et al. 2006; Best et al. 2006). In our models we consider $\beta = 0.5$ and M_{agn} as a free parameter. Note, SSS07 used AGN feedback with $\beta = 3$, but suppressed the halo formation rate instead of star formation rate as we do here.

A crucial parameter of our model is f_*/η which governs the mass to light ratio of the galaxies at any given redshift. A number of recent works have tried to measure the amount of dust obscuration of UV luminosity (parametrized here by η) at high redshifts by fitting the spectral energy distribution (SED) of LBGs (Reddy et al. 2012; Wilkins et al. 2012; González et al. 2012; Bouwens et al. 2012). They suggest a tentative evidence for the dust correction to increase with luminosity at a given redshift. However introducing such a trend, which is not yet well established (at least quantitatively), would add another source of uncertainty in our models. Therefore, for simplicity, in our models we assume η to be luminosity independent at any given redshift. It is also been suggested that the dust corrections may evolve with redshift. We do take into account this average evolution of η with z as given by Stark et al. (2009); González et al. (2012); Reddy et al. (2012). Note that for a luminosity in-

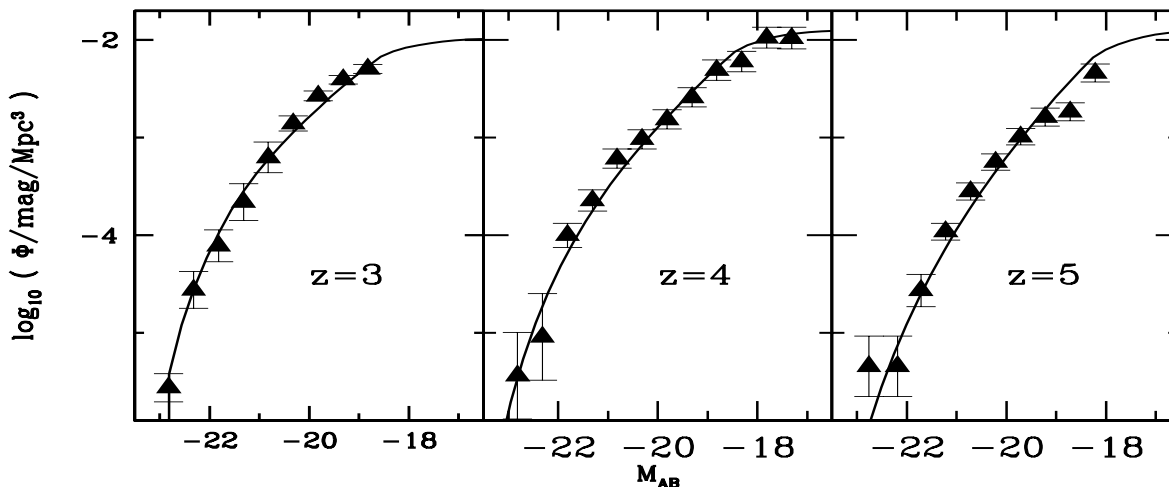


Figure 2. Comparison of observed UV LF of LBGs at three different redshifts with our best fitted model predictions. The observed data points and error bars are from Reddy et al. (2008) (for $z=3$) and Bouwens et al. (2007) (for $z=4$ & 5).

Table 1. The free parameters of our physical model.

Parameter	Description
f_*/η	Related to the light to mass ratio. This parameter is assumed to be independent of the mass of the halo.
M_{agn}	Determines the mass scale of AGN feedback. The AGN feedback is assumed to suppress the star formation in dark matter halos by a factor $(1 + M/M_{agn})^{0.5}$.
κ	Determines the typical duration of star in individual dark matter halos. The star formation rate in a halo reaches a peak value when it's age is κt_{dyn} .
Δt_0	This parameter, defined in Section 4, is used for calculating small angular scale clustering. Δt_0 is the minimum time difference between the formation epochs of a parent halo and sub-halos hosted by it.

dependent η , we only need the combined parameter f_*/η to fit the LFs of LBGs. Moreover, as we will show below, the clustering predictions are also determined solely by the combined parameter f_*/η . We describe the free parameters of our model in Table. 1.

The parameter f_*/η at each redshift is fixed by fitting the observed luminosity function of LBGs using χ^2 minimization. In this way our physically motivated model for star formation gives the relationship between the halo mass (M) and the luminosity (L) of the galaxy it hosts. It is important to note that our prescription of star formation naturally introduces a scatter in the M-L relationship because halos of mass M forming at different redshifts, produce different luminosities at the redshift of observation. SSS09 showed that this M-L relationship can successfully explain the luminosity functions of high redshift LBGs.

In Fig.2, we show the observed luminosity function of LBGs together with our best fitted model results for three different redshifts. As a fiducial model we have chosen $\kappa =$

1.0 at all redshifts and three different values for M_{agn} , $0.8 \times 10^{12} M_\odot$, $1.5 \times 10^{12} M_\odot$, and $3.0 \times 10^{12} M_\odot$ at redshifts 3, 4 and 5 respectively. With these parameters the observed luminosity functions is well reproduced for f_*/η of 0.042, 0.038 and 0.032 respectively for $z = 3, 4$ and 5. The χ^2 corresponding to the best fit luminosity function at redshifts 3, 4 and 5 are 10.80, 8.58 and 10.51 (with corresponding reduced χ^2 of 1.35, 0.78 and 1.31) respectively. These values of f_*/η are used below when we map the clustering of dark matter halos to that of galaxies.

Recent advances in multi-band deep field observations allow one to estimate SFR and stellar mass (M_*) in individual LBGs and their global stellar mass function using SED fitting. These are used to establish trends between SFR and M_* (Stark et al. 2009; González et al. 2011; Reddy et al. 2012; Wilkins et al. 2012; González et al. 2012; Bouwens et al. 2012). Note the individual values of these derived quantities need not be accurate as they depend on the models used to generate the SEDs. However, the observed trends may depend weakly on the SED model parameters. Although the focus of our paper is on LBG clustering, it would be of interest to compute these quantities and trends discussed above.

If we use the average value of $\eta \sim 4, 2.2, 2$ at $z = 3, 4, 5$ estimated from Bouwens et al. (2012); Reddy et al. (2012), we get $f_* \sim 0.17, 0.08, 0.06$ at these redshifts. This implies an increase in the fraction of baryons converted to stars with time. Using Fig. 1, we can infer that about 3 – 8% of the total baryons in a typical galaxy is converted to stars over a timescale of 300 – 500 Myr for $z = 5 - 3$.

Using the derived values of f_* we can calculate L_{UV} -stellar mass (M_*) relation from our model at any z . Our models capture a clear correlation between the two quantities as found by the previous authors (Stark et al. 2009; Labbé et al. 2010; González et al. 2010, 2011, 2012; Lee et al. 2012; Reddy et al. 2012) For example, at $z = 4$, we find a mean trend which can be approximated with a power-law $M_* \propto L_{1500}^{1.5}$. Also at $M_{AB} = -20$, we find $M_* \sim 10^9 M_\odot$.

These compare reasonably with the observations presented by González et al. (2011) (Figure 1), who find a relation $M_* \propto L_{1500}^{1.7}$, with also $M_* \sim 10^9 M_\odot$ at $M_{AB} = -20$. We can also compute the global stellar mass function for the galaxies in any luminosity range. For galaxies with absolute magnitude in the range $-18 \geq M_{AB} \geq -23$, at $z = 4$ and for $M_* \geq 10^9 M_\odot$, we find that the stellar mass function can be approximated by a powerlaw with a slope of ~ -1.5 . We also find the abundance of galaxies per dex in M_* at $10^9 M_\odot$ is about $10^{-2.2}$ per Mpc^3 . This compares reasonably well with the results of González et al. (2011) who find a slope of the stellar mass function -1.4 to -1.6 and galaxy abundance $10^{-2.5}$ per Mpc^3 per dex. We defer a detailed discussion of these issues to a future work as our focus here is on the spatial clustering of LBGs.

Thus our physically motivated models capture the basic trend seen based on SED fitting analysis. In passing we mention that the specific star formation rate (SSFR) calculated in our models and its evolution with redshifts are found to be consistent with the trends quoted in the literature (González et al. 2011, 2012; Bouwens et al. 2012). As our main focus of this work is to understand the spatial clustering of LBGs at different redshifts we defer a detailed discussion on SFR, M_* , SSFR and their redshift dependence to a future work.

3 CLUSTERING OF LBGs AT LARGE ANGULAR SCALES

We couple the semi-analytic models described above with the halo model to compute the correlation function of high- z LBGs. In order to calculate the galaxy-galaxy correlation function on all scales one requires a full knowledge of the halo occupation distribution (HOD), which describes the conditional probability $P(N|M)$ for N galaxies of a given type to reside inside a halo of mass M (Bullock et al. 2002b; Berlind & Weinberg 2002). On scales much bigger than the virial radius of a typical halo, the clustering amplitude is dominated by correlation between galaxies inside separate halos. On the other hand, on scales smaller than the typical virial radius of a dark matter halo, the major contribution to galaxy clustering is from galaxies residing in the same halo. These separate contributions to two point correlation function are called 2-halo and 1-halo terms respectively. In this section we concentrate on the 2-halo term.

The first moment of halo occupation is the mean number of galaxies of a given type inside a parent halo. It has contributions from both central and satellite galaxies (Zheng et al. 2005; Zehavi et al. 2011). In the calculation of LF in the previous section we have assumed that each halo hosts a single star forming galaxy. However, the detectability of this galaxy depends on its age, the limiting luminosity of the observations and feedback processes introduced in the previous section. Neglecting the one halo term is a good approximation for correlation functions on large scales because (i) on largest scales the clustering is insensitive to the galaxy distribution inside a halo and is dominated by the two halo term, (ii) using our model, we later show that, for the LBGs we consider, the total number of satellite galaxies of a particular luminosity is much less than the total number of central galaxies of the same luminosity in a large

volume. Thus on large scales the contribution to clustering due to satellite galaxies is not significant compared to the clustering of central galaxies.

The galaxy power spectrum on large scales (small k) due to the two halo term alone, assuming linear bias, is given by (Cooray & Sheth 2002)

$$P_g^{2h}(k, z) = b_g^2(k, z)P_{lin}(k, z), \quad (5)$$

where $P_{lin}(k, z)$ is the linear dark matter power spectrum. The scale dependent, galaxy number weighted, halo bias or in short galaxy bias, $b_g(k, z)$, is given by

$$b_g(k, z) = \frac{1}{n_g(z)} \int b(M, z)n(M, z)u(k, M, z)dM. \quad (6)$$

As before, $n(M, z)$ is the ST halo mass function, $n_g(z) = \int n(M, z)dM$ is the number density of galaxies and $b(M, z)$ is the mass dependent halo bias factor provided by the fitting function of Sheth and Tormen (Sheth & Tormen 1999; Cooray & Sheth 2002). It has the following functional form

$$b(M, z) = 1 + \frac{q\nu(M, z) - 1}{\delta_c(z)} + \frac{2p/\delta_c(z)}{1 + (q\nu(M, z))^p}, \quad (7)$$

where, $\nu(M, z) = \delta_c(z)/\sigma(M)$, $\sigma(M)$ is the linearly extrapolated rms density fluctuation on any mass scale M and $\delta_c(z)$ is the critical density required for collapse at z . Here $\delta_c(z) = D(z)\delta_c(z=0)$ with $\delta_c(z=0) = 1.686$, where $D(z)$ is the linear growth factor in a Λ CDM universe. Also we use $p = 0.3$ and $q = 0.707$ as given by Sheth & Tormen (1999). In Eq. (6) $u(k, M)$ is the Fourier transform of dark matter density profile normalized by its mass, i.e $u(k, M, z) = \bar{\rho}(k, M, z)/M$. We assume the Navarro, Frenk and White (NFW) profile (Navarro et al. 1997; Bullock et al. 2001) for the dark matter density distribution in halos. On scales much greater than the virial radius of a typical halo of mass M , $u(k, M, z) = 1$. Thus galaxy bias, $b_g(k, z)$, on large scales (much larger than the virial radius of typical collapsed halos) or small k , will be independent of k .

The actual clustering observations are for a galaxy sample with an apparent magnitude below some threshold (or a corresponding lower luminosity threshold L_{th}). So $b_g(k, z)$ in Eq. (6) should be calculated for only galaxies which have luminosity greater than L_{th} . We use our model described in Section 2 for calculating the time dependent luminosity of a galaxy hosted by a dark matter halo of mass M . This can then be used to obtain the galaxy bias for LBGs with the luminosity threshold L_{th} , at any redshift of observation z as,

$$b_g(k, L_{th}, z) = \frac{1}{n_g(L_{th}, z)} \int_0^\infty dM b(M, z)u(k, M, z) \times \int_z^\infty dz_c \Theta(L(M, z_c, z) - L_{th}) \frac{dn(M, z_c)}{dz_c}. \quad (8)$$

Here, $L(M, z_c, z)$ is the luminosity of a galaxy of mass M at z , formed at z_c . The theta function, $\Theta(L(M, z_c, z) - L_{th})$, in the above equation ensures that the galaxy bias will have contribution only from those galaxies formed at z_c and that shine above the threshold luminosity L_{th} at z . If we do not have this constraint imposed by the Θ function, the integral over z_c is just $\int_z^\infty dz_c dn(M, z_c)/dz_c = n(M, z)$ and the Eq. (8) reduces back to Eq. (6). Also $n_g(z, L_{th})$ is the number density of galaxies having luminosity in excess of the

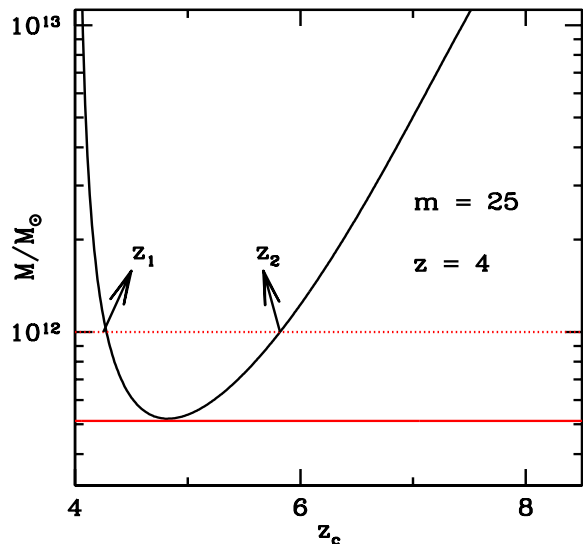


Figure 3. Masses of the dark matter halos that shine with an apparent magnitude $m = 25$ (or absolute magnitude $M_{AB} = -21.1$) at $z = 4$ as a function of their formation (collapse) redshift. We can clearly see that halos of a particular mass formed at two different redshifts can shine with the same brightness at $z = 4$. We refer these two redshifts as z_1 and z_2 . For example, when $M = 10^{12} M_\odot$ (shown by dotted red horizontal line) these two redshifts are approximately 4.27 and 5.82. The figure also shows the minimum mass of the galaxy that can produce an apparent magnitude 25 at $z = 4$ (in red horizontal solid line). This mass is roughly $5.2 \times 10^{11} M_\odot$ and is formed at $z_c \sim 4.8$.

limiting luminosity, L_{th} , and is given by,

$$n_g(L_{th}, z) = \int_0^\infty dM \int_z^\infty dz_c \Theta(L(M, z_c, z) - L_{th}) \times \frac{dn(M, z_c)}{dz_c}. \quad (9)$$

In our prescription of star formation, at any given redshift z , a galaxy hosted by a halo of mass M will shine with a given luminosity at two different ages, when its star formation is either in the rising phase or in the declining phase. As a result there are two redshifts of formation $z_1(L_{th}, M, z)$ and $z_2(L_{th}, M, z)$, such that the galaxy will produce an observed luminosity L_{th} at z . We demonstrate this in Fig. 3, where we have plotted the halo mass M that can host a galaxy of luminosity L_{th} (corresponding to an apparent magnitude $m = 25$) at $z = 4$ against the redshift of formation of the halo. The figure clearly shows that halos of any mass (above a minimum mass M_{min}) formed at two different redshifts can shine with the same luminosity at $z = 4$. For example, when $M = 10^{12} M_\odot$ these two redshifts are approximately 4.27 and 5.82 (shown by the abscissa of intersection of the horizontal red dotted line with the curve). A halo of mass $10^{12} M_\odot$ formed between these redshifts will shine with a magnitude brighter than $M_{AB} = -20.1$ at $z = 4$. For the case illustrated above, this minimum mass is roughly $5.2 \times 10^{11} M_\odot$ and this halo has to be formed at $z_c \sim 4.8$ for it to have a luminosity L_{th} at $z = 4$. In our models, the exact values of z_1 , z_2 and M_{min} for a given observed luminosity will depend only on f_*/η that we fix by fitting the luminosity function as discussed before.

Table 2. Asymptotic values of $b_g(L_{th}, z)$ predicted uniquely by using model parameters that best fit the high z LFs. These parameters are (i) f_*/η , an indicator of the light to mass ratio at any redshift (ii) $M_{min}(L_{th}, z)$, the minimum mass of a galaxy that can shine brighter than a given luminosity threshold L_{th} at redshift of observation, (iii) $n_g(z, L_{th})$, the number density of galaxies with luminosity greater than L_{th} in units of $10^{-4}(h/Mpc)^3$ and $b_g(L_{th}, z)$, the luminosity dependent galaxy bias are tabulated for three limiting apparent magnitudes at each redshift. The last column is the galaxy bias given by Hildebrandt et al. (2009), after correcting for the larger σ_8 adopted by them.

z	f_*/η	m	M_{AB}	M_{min}/M_\odot	n_g	b_g	$b_g(H)$
3	0.042	24.5	-21.1	7.6×10^{11}	5.81	3.63	4.50
		25.0	-20.6	4.2×10^{11}	14.2	3.23	3.22
		25.5	-20.1	2.5×10^{11}	30.3	2.92	2.67
4	0.038	25.0	-21.1	5.2×10^{11}	3.66	4.69	5.14
		25.5	-20.6	3.1×10^{11}	9.17	4.22	4.25
		26.0	-20.1	2.0×10^{11}	20.8	3.82	3.51
5	0.032	25.5	-21.0	4.0×10^{11}	1.56	5.95	7.81
		26.0	-20.5	2.5×10^{11}	4.32	5.36	6.08
		26.5	-20.0	1.5×10^{11}	10.8	4.90	5.09

Our model of star formation ensures that halos of mass $M > M_{min}$ collapsing between $z_1(L_{th}, M, z)$ and $z_2(L_{th}, M, z)$ will always shine brighter than L_{th} at z , while galaxies formed outside these intervals do not. Thus the Θ function in Eq. 8, is unity for $M > M_{min}$ and $z_1 \leq z_c \leq z_2$ and zero otherwise. Therefore $b_g(k, L_{th}, z)$ in Eq. (8) can be written as,

$$b_g(k, L_{th}, z) = \frac{1}{n_g(L_{th}, z)} \int_{M_{min}}^\infty dM b(M, z) u(k, M, z) \int_{z_2}^{z_1} dz_c \frac{dn(M, z_c)}{dz_c}. \quad (10)$$

At this point, given M_{min} , z_1 and z_2 one can compute $b_g(k, L_{th}, z)$. As these parameters can be fixed by the parameters governing the star formation in a halo, the observed luminosity function alone in principle will allow us to predict $b_g(k, L_{th}, z)$ uniquely.

We present our results for the fiducial set of model parameters that reproduces the observed luminosity function. In Table 2 we present the predicted asymptotic ($k \rightarrow 0$) value of $b_g(L_{th}, z)$ at three different redshifts (and three luminosity ranges each) using f_*/η values obtained by fitting the observed luminosity function of LBGs at these redshifts. This table also gives apparent magnitude cut-off (m), corresponding absolute magnitude cut-off (M_{AB}), M_{min} and $n_g(L_{th}, z)$ as given in Eq. 8.

We compute the luminosity dependent galaxy power spectrum, $P_g^{2h}(k, L_{th}, z)$, by substituting $b_g(k, L_{th}, z)$ from Eq. (10) into Eq. (5). We then have

$$P_g^{2h}(k, L_{th}, z) = b_g^2(k, L_{th}, z) P_{lin}(k, z). \quad (11)$$

The corresponding luminosity dependent two point correlation function of galaxies with luminosity greater than L_{th} at z , can now be calculated using (Peebles 1980)

$$\xi_g^{2h}(r, z, L_{th}) = \int_0^\infty \frac{dk}{2\pi^2} k^2 \frac{\sin(kr)}{kr} P_g^{2h}(k, z, L_{th}). \quad (12)$$

We compute luminosity dependent angular correlation func-

tion $w(\theta, z)$ from the spatial correlation function using Limber equation (Peebles 1980)

$$w(\theta, z) = \int_0^\infty dz' N(z') \int_0^\infty dz'' N(z'') \xi_g(z, r(\theta; z', z'')) \quad (13)$$

where $r(\theta; z', z'')$ is the comoving separation between two points at z' and z'' subtending an angle θ with respect to an observer today. Here we have also incorporated the normalized redshift selection function, $N(z)$, of the observed population of galaxies. In Eq. (13) we neglect the redshift evolution of clustering of the galaxies detected around z . Hence the spatial two-point correlation function $\xi_g(r, z)$ is always evaluated at the observed redshift.

In Fig. 4 we over plot the angular correlation function computed in this way using the predicted value of b_g from our models that produce best fits to the LF, on the observed angular two point correlation functions given by Hildebrandt et al. (2009). We have also plotted the angular correlation function of dark matter density (obtained by putting $b_g(k, L_{th}, z) = 1$) in dotted-blue curves. To compute our correlation function we used the $N(z)$ from Hildebrandt et al. (2009), which are kindly provided by the authors (*BC_{sim}* redshift distribution; see Table 4 and Figure 5 of the paper). It is clear that at large angular scales (i.e $\theta \geq 80''$), where the linear approximation used here is valid, our model predictions match well with the observations at different redshifts and different luminosity (or apparent magnitude) thresholds.

The large scale galaxy bias is determined by Hildebrandt et al. (2009) from their data by making power law fits to observed galaxy correlation functions, and comparing the corresponding galaxy variance at $8h^{-1}$ Mpc ($\sigma_{8,g}$) with σ_8 computed from the dark matter power spectrum. In the last column (column 7) of Table. 2 we show the large scale bias $b_g(H)$ of LBGs obtained this way by Hildebrandt et al. (2009), after correcting for the larger σ_8 adopted by them. The large scale bias b_g that we predict from our models agrees well with $b_g(H)$ estimated by Hildebrandt et al. (2009) from their power law fit, for all but the brightest of the LBG samples. For the brightest sample of LBGs at all redshifts the bias we predict is systematically lower. Nevertheless, in agreement with Hildebrandt et al. (2009), we also find that (i) at a given z the bias increases with increasing luminosity and (ii) for a given L_{th} the bias increases with increasing z . However at any given z the spread in b_g as a function of L_{th} is less in our case compared to that of Hildebrandt et al. (2009).

We also see from Fig. 4 that the two halo term is not able to account for the strength of clustering seen on small angular scales given by $\theta < 50''$ at redshift 3 and $\theta < 80''$ at redshifts 4 and 5. However we have not yet included the 1-halo term in the correlation function, arising from correlation between galaxies within any given halo. We will address this issue in the Section 4.

3.1 Sensitivity of large angular scale correlation function to change in parameters

Here we present the sensitivity of the predicted large scale correlation functions to changes in astrophysical and cosmological parameters. To do this, we considered models, where

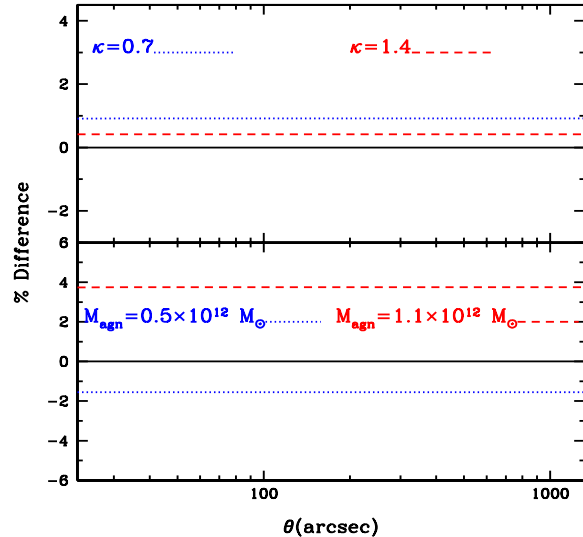


Figure 5. The percentage change in angular correlation function when one varies κ (top panel) and M_{agn} (bottom panel) around the fiducial model at $z = 3$. Here the plots are for threshold apparent magnitude 25. For each value of κ and M_{agn} we use the appropriate f_*/η values that best fit the observed luminosity function.

a single astrophysical or cosmological parameter is assigned values around its fiducial value, keeping all other parameters fixed to their fiducial value.

3.1.1 Sensitivity to Astrophysics

We begin by showing in Fig. 5 the sensitivity of large scale clustering predictions to the assumed values of κ , which determines the duration of star formation in a halo, and M_{agn} , a characteristic mass scale corresponding to the AGN feedback. Note that, in each case, the f_*/η gets automatically fixed when we fit the observed luminosity function. The results are shown at $z = 3$ and $m = 25$. Any change in astrophysical parameters will not alter the amplitude and shape of the dark matter correlation function. However, in principle, they can change the luminosity-dependent galaxy bias by simply changing the luminosity of a galaxy. Hence, on large scales, the astrophysical parameters will affect clustering predictions only through galaxy bias.

As we can see explicitly in Fig. 5, the changes in astrophysical parameters produce negligible effects on the clustering on large scales. This is expected for M_{agn} because of the following reason. For $z = 3$, we have chosen the parameter $M_{agn} \sim 0.8 \times 10^{12} M_\odot$, so that the predicted LF matches with the observed data. In the plot, we varied M_{agn} between $0.5 \leq M_{agn}/10^{12} M_\odot \leq 1.1$. From Table 2, it is clear that M_{min} , the minimum mass cutoff in the integral to calculate large scale bias (see Eq. 10), is always less than $10^{12} M_\odot$. Since the number density of halos decays exponentially with $\sigma^2(M)$ at these mass scales, the major contribution to $b_g(z, L_{th})$ in Eq. 10 comes from mass scales lower than M_{agn} . Therefore, we can conclude that the value of M_{agn} and hence the AGN feedback used in our models will not be that sensitive to clustering on large scales.

From Fig. 5, it is also clear that the change in κ is not af-

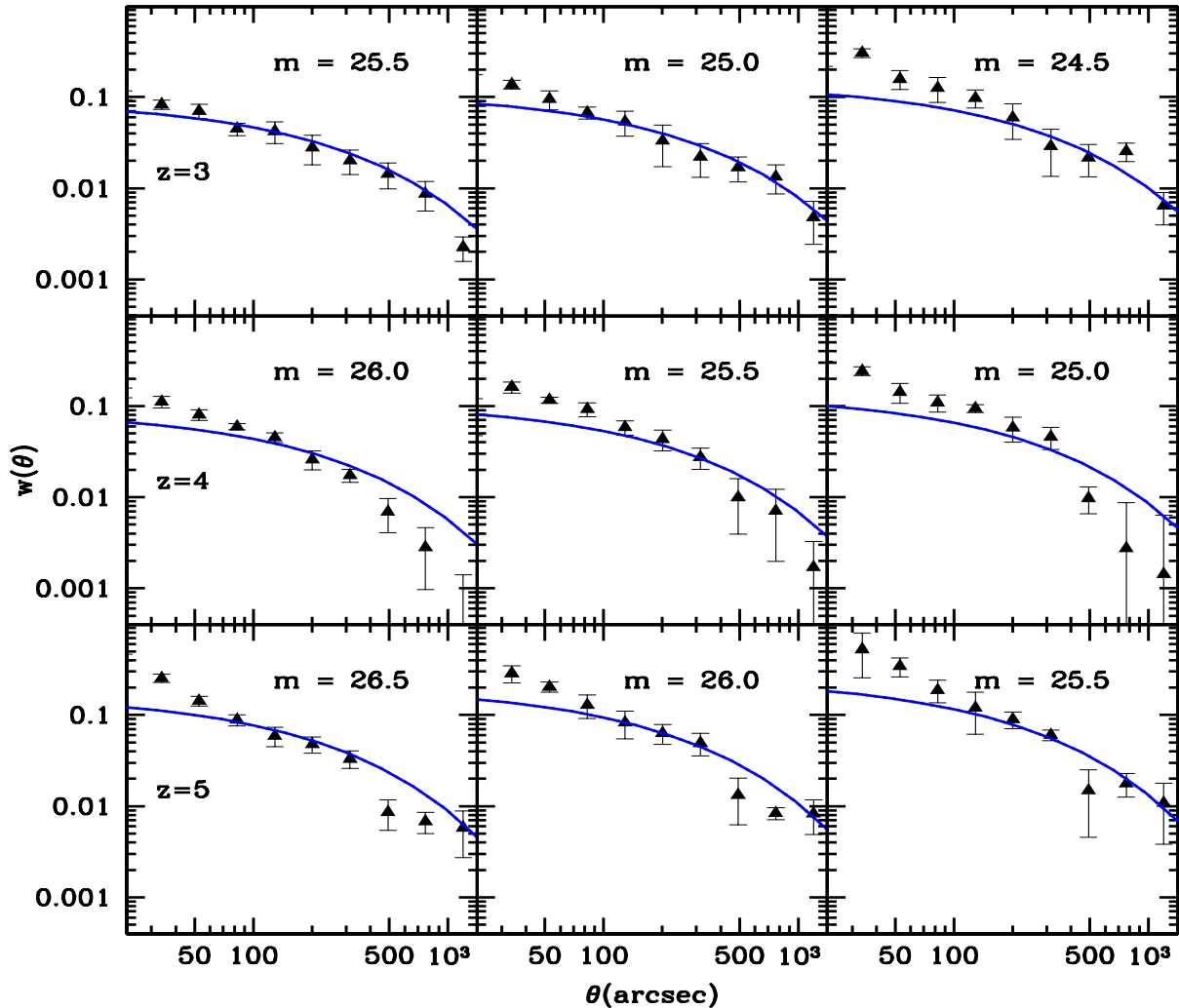


Figure 4. The large scale angular correlation function of LBGs at redshifts 3, 4 and 5 for various limiting magnitudes. Each row corresponds to a particular redshift, which is labelled in the first panel of that row. In each row there are three panels showing the clustering predictions for three limiting galaxy magnitudes that are labelled in each panel. The blue solid curves are our model predictions of galaxy angular correlation functions. Also shown in blue dotted lines are the angular correlation functions of dark matter density. The data points and error bars shown by black triangles are from Hildebrandt et al. (2009).

fecting the predicted clustering at large scales. We know that a change in κ is not affecting the number density of halos of a particular mass. However a smaller κ means the baryons are converted to stars over a shorter timescale. Hence for a fixed f_* (or the baryon fraction being converted to stars), a smaller κ leads to an increase in the SFR and increased luminosity. This will shift the predicted total LF more or less along the luminosity axis. While fitting the observed luminosity function this shift with respect to our fiducial model is nullified by changing f_*/η . This means that even when the κ is decreased and the star formation rate is enhanced, the observed luminosity of a galaxy hosted by a halo of a given mass is almost unchanged, and hence the luminosity dependent large scale clustering is not significantly affected.

3.1.2 Sensitivity to Cosmology

On large scales values of cosmological parameters can affect two point correlation function by changing the amplitude and shape of dark matter power spectrum and also by modifying the halo mass function and halo bias and thereby altering the galaxy bias. To see these effects more clearly, we have plotted in Fig. 6 the percentage differences in the clustering predictions with changes in cosmological parameters from their fiducial value. In this figure we varied the cosmological parameters within their 2σ limits determined by WMAP7 year data. The parameter f_*/η in each case is fixed by fitting the observed luminosity function. All the curves in Fig. 6 are for $z = 3$ and threshold apparent magnitude 25. The parameter values which are different from the fiducial value are shown in each panel of Fig 6. The percentage

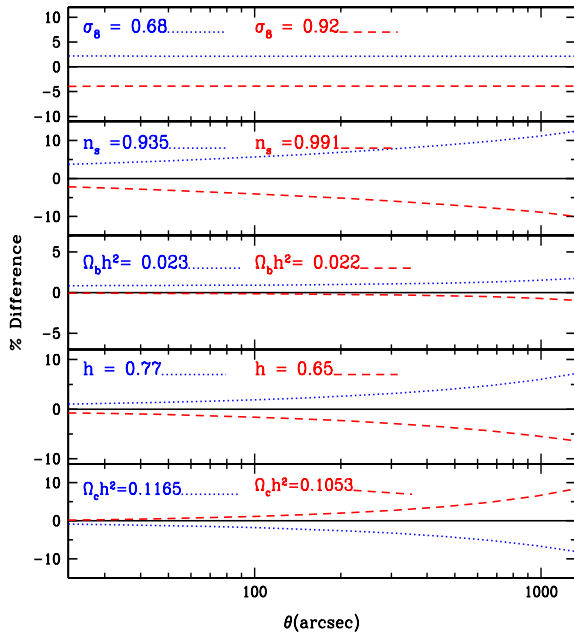


Figure 6. The percentage change in angular correlation function when one varies the cosmological parameters around the fiducial model at $z = 3$. Here the plots are for threshold apparent magnitude 25. In each case, f_*/η values are varied to consistently reproduce the observed luminosity function.

difference of clustering ranges from minimum of few % (for σ_8 and Ω_b) and a maximum of $\sim 12\%$ (for n_s) for the assumed values of parameters, with notable differences being produced only on very large scales.

We are particularly surprised why our models with various values of σ_8 predict almost same large scales clustering. In order to understand this we consider two models A and B with different values of σ_8 given by $\sigma_8^A = 0.68$ and $\sigma_8^B = 0.80$. In Appendix A we have obtained an expression for the approximate ratio between galaxy correlation functions of models A and B on large scales (Eq. A7). In particular we consider the clustering of galaxies with threshold apparent magnitude 25. From our analysis in Section 4 we can obtain the average mass of a galaxy, M_{av} , that can shine brighter than this magnitude threshold. For models A and B, the corresponding average masses are $M_{av}^A \sim 5.6 \times 10^{11} M_\odot$ and $M_{av}^B \sim 10^{12} M_\odot$ respectively. Using these in Eq. A7 we get the ratio between correlation functions on large scales for models A and B to be 1.05. This is consistent with our model predictions shown in Fig. 6. Thus in our model various effects due to the change in σ_8 cancel each other to get similar large scale clustering of high redshifts LBGs.

4 THE CORRELATION FUNCTIONS INCLUDING THE SATELLITES

In the previous sections we assumed that a halo can host at most one detectable galaxy. This assumption is not adequate to explain clustering at small angular scales, especially on scales smaller than virial radius. Each halo can

in principle host multiple galaxies. A complete description of the distribution of galaxies inside a halo is called halo occupation distribution (HOD). Following the approach of Kravtsov et al. (2004) we separate the central and satellite contributions to HOD (see also Zheng et al. (2005); Cooray & Ouchi (2006); Conroy et al. (2006)). That is the mean number of galaxies inside a dark matter halo can be written as $N_g(M) = f_{cen}(M) + N_s(M)$ where $f_{cen}(M)$ and $N_s(M)$ are respectively the mean number of central and satellite galaxies. We also assume the central galaxy to be situated at the center of the halo and satellite galaxies around it (Kravtsov et al. 2004). In this approach the 1-halo term has contributions from the correlation between central-satellite and satellite-satellite pairs.

In the framework of this approach, the the total correlation function can be written as (Cooray & Sheth 2002)

$$\xi_g(r) = \xi_g^{1h}(r) + \xi_g^{2h}(r) \quad (14)$$

where each term on RHS has contributions from central as well as satellite galaxies.

4.1 The HOD: a physical model

Often the HOD is modelled in a parametrized form, motivated by simulations or observations, and the value of the parameters are derived by fitting the galaxy correlation function. Instead we adopt a more physical approach. We ask, given our model for galaxy formation, what is the expected mean occupation number of central and satellite galaxies of a given luminosity, in a given halo. These can then be used to compute the correlation function.

4.1.1 The central galaxy occupation

We begin by formally expressing the mean occupation number of central galaxies with a luminosity threshold L_{th} inside a halo of mass M at any redshift z . This is given by,

$$\begin{aligned} f_{cen}(L_{th}, M, z) &= \frac{\int_z^\infty \frac{dn(M, z_c)}{dz_c} \Theta(L(M, z, z_c) - L_{th}) dz_c}{\int_z^\infty dz_c \frac{dn(M, z_c)}{dz_c}} \\ &= \frac{\int_{z_1}^{z_2} dz_c \frac{dn(M, z_c)}{dz_c}}{n(M, z)}. \end{aligned} \quad (15)$$

Thus, in our model $f_{cen}(L_{th}, M, z)$ is the probability that a halo of mass M at z hosts a galaxy with brightness greater than L_{th} . Again the $\Theta(L_{th}(M, t(z)) - t(z_c))$ function ensures that only those galaxies collapsing at z_c and having $L > L_{th}$ at z are counted in the integral over z_c . As described earlier, $z_1(M, L_{th}, z)$ and $z_2(M, L_{th}, z)$ are the two redshifts at which a galaxy of mass M has to be formed, so that it shines with an observed luminosity L_{th} at z .

In Fig. 7 we have plotted as thin lines, the average occupation number of central galaxies ($f_{cen}(M)$) as function of the mass of the parent halo, calculated using the above prescription. The results are shown at $z = 3, 4$ and 5 for three different magnitude thresholds which are labelled in each panel. These curves are obtained using the fiducial set of model parameters (given in Section 2) that reproduce the

observed luminosity function¹. We can see that for a given redshift and limiting magnitude $f_{cen}(M)$ increases with the mass of the hosting halo to a limiting value of 1. Also note that the mean occupation number of central galaxies drops to zero below some mass scale M_{min} . This value of M_{min} is almost the same as that given in Table. 2; the change is due to the minor corrections to f_*/η we apply to take care of the satellite contribution to the LF in Section 4.4. In Table 3 we give the values of M_{min} for all the three redshifts and limiting magnitudes. For example, at $z = 4$ for apparent magnitudes 25, 25.5 and 26, $M_{min} = 5.7 \times 10^{11}$, 3.4×10^{11} and $2.1 \times 10^{11} M_\odot$ respectively. Many of the semi analytical models for clustering of low redshift galaxies (Zehavi et al. 2011; More et al. 2009) use a step like function with smooth cut-off profile for $f_{cen}(M)$. One can see from Fig. 7 that such a profile for $f_{cen}(M)$ naturally arises from our simple physical model of star formation. Infact the smoothness of the cut-off seen in the function $f_{cen}(M)$ at the low mass end for our models, is due to the scatter in the M-L relationship.

It is of interest to calculate the average value of f_{cen} for halos above the threshold mass M_{min} , defined as

$$\langle f_{cen} \rangle(L_{th}, z) = \frac{\int_{M_{min}}^{\infty} dM f_{cen}(M, z) n(M, z)}{\int_{M_{min}}^{\infty} dM n(M, z)}. \quad (16)$$

We give the value of $\langle f_{cen} \rangle$ in Table 3 for different magnitude thresholds and redshifts. One can see from Table 3 that $\langle f_{cen} \rangle$ is generally of order 0.4; or 40% of halos above M_{min} can typically host luminous LBGs, for any given luminosity threshold and redshift. This number, which in our model only depends on f_*/η obtained by a fit to the LFs, is comparable to the duty cycle values preferred by Lee et al. (2009, 2012).

Finally we also give in Table 3, the average mass M_{av} of a halo hosting the central LBG, for each redshift and luminosity threshold. This average mass is defined by,

$$M_{av} = \frac{\int_0^{\infty} dM M f_{cen}(M, z) n(M, z)}{\int_0^{\infty} dM f_{cen}(M, z) n(M, z)}. \quad (17)$$

At $z = 4$ and for apparent magnitudes 25, 25.5 and 26, $M_{av} = 10^{12}$, 6.2×10^{11} and $3.9 \times 10^{11} M_\odot$ respectively. At $z = 5$ these masses are smaller by a factor ~ 1.4 while at $z = 3$, M_{av} is larger by a similar factor.

We also note that $b_g(k, L_{th}, z)$ in Eq. (10) can be rewritten in terms of $f_{cen}(L_{th}, M, z)$ as,

$$b_g(k, L_{th}, z) = \frac{1}{n_g(L_{th}, z)} \int_0^{\infty} dM n(M, z) b(M, z) \times f_{cen}(L_{th}, M, z) u(k, M, z) \quad (18)$$

which is the standard formula for the galaxy bias, excluding the satellite contribution.

4.1.2 The satellite galaxy occupation

In order to get an estimate of the number of subhalos and thereby the number of satellite galaxies hosted by a halo

of mass M , we use the conditional or progenitor mass function. The conditional mass function gives the comoving number density of subhalos of mass M_s which formed at z_s inside a region containing a mass M (or comoving volume V) that have a non-linear over density δ at z_p . It is given by (Mo & White 1996; Cooray & Sheth 2002)

$$\bar{n}(M_s, z_s | M, \delta, z_p) dM_s = \frac{\rho_m}{M_s} \nu_{10} f(\nu_{10}) \frac{d\nu_{10}}{\nu_{10}} \quad (19)$$

where

$$\nu_{10} = \frac{(\delta_c(z_s) - \delta_l(\delta, z_p))^2}{\sigma^2(M_s) - \sigma^2(M)}. \quad (20)$$

Here, $\delta_l(\delta, z_p)$ is the linear density contrast at redshift z_p corresponding to non-linear over density δ and $\rho_m = \Omega_m \rho_c$ is the back ground density of baryons and cold dark matter. It should be noted that the formation epoch of the subhalo should precede the formation epoch of the parent halo ($z_s > z_p$) and mass of the subhalo should be always smaller than that of the parent halo ($M > M_s$). The function on the RHS of Eq. (19) has the same form as the unconditional mass function but with $\delta_c^2(z_s)/\sigma^2(M)$ being replaced by $(\delta_c(z_s) - \delta_l(\delta, z_p))^2/(\sigma^2(M_s) - \sigma^2(M))$. We use Sheth-Tormen form for the RHS in Eq. (19), in our calculations (see Section 3.3 of Cooray & Sheth (2002) for more details). The total number of halos of mass M_s which formed at z_s inside the volume containing mass M is

$$N(M_s, z_s | M, \delta, z_p) dM_s = (M/\rho_m) \bar{n}(M_s, z_s | M, \delta, z_p) dM_s, \quad (21)$$

where we have multiplied \bar{n} by the comoving volume (M/ρ_m) .

Our aim is to find the number of satellite galaxies of a particular luminosity inside a dark matter halo of mass M . To calculate this we assume that the region containing mass M is a collapsed dark matter halo at z . Thus in Eq. (19) we take $\delta_l(\delta, z_p) = \delta_c(z_p)$ (Cooray & Sheth 2002). In this limit the conditional mass function gives the number density of satellite halos in the mass range M_s and $M_s + dM_s$ at z_c inside a halo of mass M that collapsed at z . We choose the time derivative of $N(M_s, z_c | M, \delta, z)$ as the formation rate of subhalos of mass M_s inside a big halo of mass M . We also assume that even though dark matter halos are formed and destroyed inside the over dense cell of mass M , the satellite galaxies formed in these subhalos have survived and can be observed.

We further assume that no subhalo should be formed very close to the formation epoch of parent halo. More precisely if $t_p = t(z_p)$ is the age of the universe when a parent halo collapsed then all the subhalos formed inside that parent halo within a time interval Δt_0 prior to t_p do not host a satellite galaxy; rather they will be part of the parent halo itself. Thus we assume $t_p - t_s \geq \Delta t_0$ where $t_s = t(z_s)$ is the age of the universe when the sub halo formed inside a parent halo. In our models we vary Δt_0 as a free parameter. Also we expect that it is of the order of dynamical time scale t_{dyn} of the parent halo. It should be noted that the time scale Δt_0 corresponds to a redshift interval Δz_0 which is a function of the redshift of collapse of the parent halo².

¹ Inclusion of the contribution of satellite galaxies slightly modifies the luminosity function and hence the best fit f_*/η (see Section 4.4). In all the subsequent calculations we use this new best fit f_*/η .

² We have also explored an alternate scheme whereby halos of satellite galaxies must have a mass smaller than the parent halo

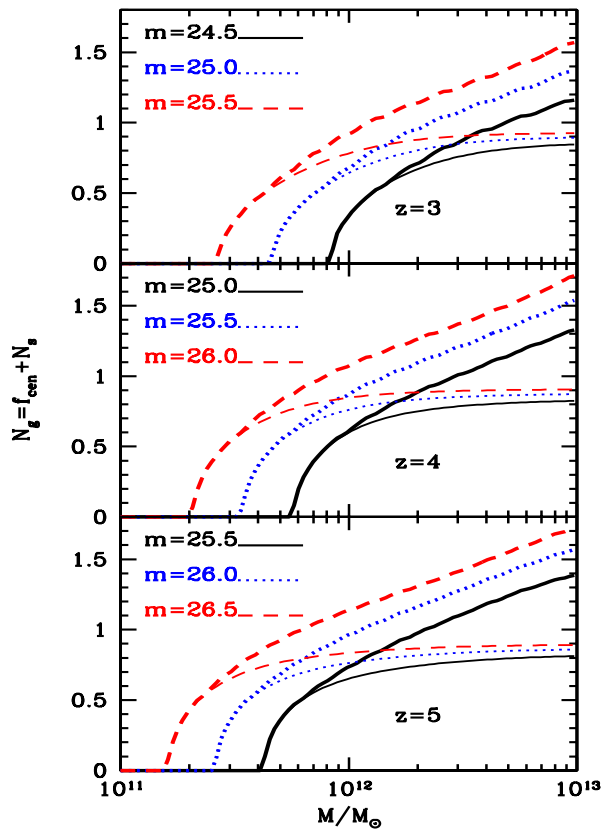


Figure 7. The halo occupation distribution, $\langle N_g(M) \rangle$, as a function of the mass of the hosting halo, as predicted by our models at various redshifts for three limiting magnitudes. In each panel the thin curves corresponds to $f_{cen}(M)$ where as the thick curves give the total occupation $N_g(M) = f_{cen}(M) + N_s(M)$. The redshifts and apparent magnitudes are labelled in each panel. The curves are obtained using a fiducial set of model parameters (given in Section 2) that reproduce the observed luminosity function. In addition to that, to obtain the satellite occupation ($N_s(M)$), we have adopted $\Delta t_0 = 1.6t_{dyn}, 1.5t_{dyn}$ and $1.4t_{dyn}$ at $z = 3, 4$ and 5 respectively (see text for details).

In principle, a parent halo seen at z could itself have collapsed at a slightly earlier redshift $z_p > z$. However, it turns out (see Fig. 7), that only massive halos with $M \geq 10^{12} M_\odot$ have significant probability of hosting an observable satellite galaxy. Such massive halos are more likely to collapse close to the redshift of observation z itself (as their formation rate will rapidly fall with increasing z_p). Thus for simplifying our computations of the satellite occupation, we will assume that the collapse redshift of the parent halo is also the redshift of observation; i.e $z_p = z$. Of course for computing f_{cen} we do not make any such approximation.

In the following discussions we also assume that star

by a factor f_m (same as the parameter φ in Lee et al. (2009)). Since smaller mass halos typically collapse earlier than larger masses, the parameter Δt_0 used here achieves a similar goal to f_m ; although it does not exclude similar but slightly smaller mass satellites in the main parent halo.

formation models for the central and satellite galaxies are identical (given by Eq. (1)). This is similar to the assumption used by previous authors (Lee et al. 2009; Berrier et al. 2006; Conroy et al. 2006) where feedback due to halo merging processes are ignored.

We first compute the number of satellite galaxies of magnitude in the range M_{AB} and $M_{AB} + dM_{AB}$ inside a halo of mass M . This is given by,

$$\varphi(M, M_{AB}, z) dM_{AB} = \int_{z-\Delta z_0}^{\infty} \frac{dN(M_s, z_s | M, z)}{dz_c} \times \frac{dMs}{dL_{1500}} \frac{dL_{1500}}{dM_{AB}} dM_{AB} dz_c. \quad (22)$$

It should be noted that $\varphi(M, M_{AB}, z) dM_{AB}$ is not the luminosity function of satellite galaxies, but the total number of satellite galaxies in a magnitude range M_{AB} and $M_{AB} + dM_{AB}$ inside a halo of mass M . The average number of satellites, N_s , with luminosity greater than L_{th} in halo of mass M at redshift z can be computed as

$$\langle N_s | L_{th}, M, z \rangle = \int_{L_{th}}^{\infty} \varphi(M, L, z) dL \quad (23)$$

where the luminosity L is related to M_{AB} in the standard manner.

4.1.3 The total halo occupation

We have plotted in Fig. 7 the total occupation number of galaxies, $N_g(M) = f_{cen}(M) + N_s(M)$, as a function of the mass of the parent halo. These curves are shown in thick lines for at $z = 3, 4$ and 5 and for three luminosity thresholds. Thin lines correspond to occupation number of central galaxies. In order to obtain $N_s(M)$, apart from the fiducial model parameters that fit the observed luminosity function, we have adopted $\Delta t_0 = 1.6t_{dyn}, 1.5t_{dyn}$ and $1.4t_{dyn}$ at $z = 3, 4$ and 5 respectively. These values of Δt_0 are chosen as they are later used in Section 5.1 for explaining the small angular scale clustering. We find that for each limiting magnitude the mean number of satellites is a monotonically increasing function of hosting halo mass. As an example at $z = 4$ for a halo of mass $2 \times 10^{12} M_\odot$ the mean satellite occupation numbers are respectively 0.14, 0.27 and 0.38 at threshold apparent magnitudes of 25, 25.5 and 26. For a bigger halo of mass $5 \times 10^{12} M_\odot$ these numbers change to 0.34, 0.48 and 0.61 for the same limiting magnitudes at the same redshift.

We have also computed the average value of N_s in a manner similar to calculating $\langle f_{cen} \rangle$ in Eq. (16). The results are given in the last column of Table 3. We see from the table that typically $\langle N_s \rangle$ is only about 5-10% of $\langle f_{cen} \rangle$. Thus the average number of detectable satellites, in a halo, is typically much less than unity. This implies that all halos do not necessarily host an additional detectable satellite galaxy; however some small fraction of them do and it is these pairs of LBGs which contribute to the small scale clustering. Such a conclusion has also been arrived at by Conroy et al. (2006) using numerical simulations.

It is also of interest to ask for a characteristic mass M_P of a parent halo which is hosting a detectable satellite galaxy.

We define this as follows:

$$M_P = \frac{\int_0^\infty dM MN_s(L_{th}, M, z)n(M, z)}{\int_0^\infty dMN_s(L_{th}, M, z)n(M, z)} \quad (24)$$

This is also given in Table 3. For apparent magnitudes 25, 25.5 and 26, and $z = 4$, $M_P = 1.9 \times 10^{12} M_\odot$, $1.2 \times 10^{12} M_\odot$ and $7.4 \times 10^{11} M_\odot$ respectively. For $z = 3$ the corresponding M_P is ~ 1.5 times larger, while for $z = 5$, M_P is smaller by a factor ~ 1.4 . This also means that the characteristic mass of parent halos hosting detectable satellites is ~ 2 times larger than the mass of the halo hosting a central LBG.

Note that the mean satellite number obtained in our physically motivated models can be fit asymptotically by a power law of the form $N_s(M) \propto M^\alpha$, with $\alpha \sim 0.6 - 0.9$. Interestingly this is similar to the parametrized form $N_s(M)$ used in Hamana et al. (2006), who also adopt a similar slope. Moreover, the form of HOD that we derive from our physically motivated model (and shown in Fig. 7) is also similar to that obtained by Conroy et al. (2006) from their models of HOD using N-body simulations combined with a prescription of associating mass to light (see Figures 8 and 10 of their paper).

4.2 The one halo term

We can now compute the 1-halo term using the standard assumption that radial distribution of satellite galaxies inside a parent halo follow the dark matter density distribution (Cooray & Sheth 2002). For the present calculations we use the NFW form for the dark matter density distribution. In this case the 1-halo term is given by (Tinker et al. (2005); Cooray & Ouchi (2006); see also Skibba & Sheth (2009))

$$\xi^{1h}(L_{th}, R, z) = \frac{1}{(n_g^T)^2} \int dM n(M, z) \times \left[2f_{cen}(L_{th}, M, z) \langle N_s | L_{th}, M, z \rangle \frac{\rho_{NFW}(R|M)}{M} + \langle N_s(N_s - 1) | L_{th}, M, z \rangle \frac{\lambda_{NFW}(R|M)}{M^2} \right]. \quad (25)$$

Here,

$$n_g^T(L_{th}, z) = \int dM n(M, z) (f_{cen}(M, z) + \langle N_s | L_{th}, M, z \rangle) \quad (26)$$

is the total number density of galaxies which includes both the central and satellite galaxies. Further ρ_{NFW} is the NFW profile of dark matter density inside a collapsed halo and $\lambda_{NFW}(r|M)$ is the convolution of this density profile with itself (Sheth et al. 2001). The NFW density profile is given by

$$\rho_{NFW}(M, R) = \frac{4\rho_s}{(R/R_s)(1 + R/R_s)^2} \quad (27)$$

where the ρ_s and R_s are characteristic density and radius respectively. The ratio of the virial radius and the characteristic radius of the halo is defined as the concentration parameter ($c = R_{vir}/R_s$). For the halo concentration parameter we use the fitting functions given by Prada et al. (2012) (Eq. (14-23) of their paper). These fitting functions of concentration parameter at high redshifts, unlike earlier fits, flatten and then upturn with increasing mass. We also check the sensitivity of our results to other expressions for

Table 3. Physical parameters constrained using observed luminosity function of high- z LBGs after incorporating the satellite galaxies in our semi-analytical models. These parameters are f_*/η , an indicator of the light to mass ratio at any redshift, $M_{min}(L_{th}, z)$, the minimum mass of a galaxy that can shine brighter than a given luminosity threshold L_{th} at redshift of observation, $M_{av}(L_{th}, z)$ is the average mass of a dark matter halo that can host a central LBG satisfying the luminosity threshold L_{th} , $M_P(L_{th}, z)$ the characteristic mass of a parent dark matter halo that hosts satellite LBGs which satisfy the luminosity threshold L_{th} , $\langle f_{cen} \rangle$, the average central occupation and $\langle N_s \rangle$, the average satellite occupation.

z	f_*/η	m	$\frac{M_{min}}{10^{11} M_\odot}$	$\frac{M_{av}}{10^{11} M_\odot}$	$\frac{M_P}{10^{11} M_\odot}$	$\frac{\langle f_{cen} \rangle}{10^{-2}}$	$\frac{\langle N_s \rangle}{10^{-2}}$
3	0.040	24.5	8.2	15.7	30.0	40.1	2.2
		25.0	4.6	9.2	18.0	39.1	3.0
		25.5	2.7	5.6	11.1	39.2	3.8
4	0.035	25.0	5.7	10.0	18.8	40.0	2.5
		25.5	3.4	6.2	11.7	40.3	3.0
		26.0	2.1	3.9	7.4	42.6	3.8
5	0.030	25.5	4.2	7.0	12.2	38.7	2.6
		26.0	2.6	4.5	7.7	41.5	3.3
		26.5	1.6	2.9	5.0	42.5	3.8

concentration parameter. Also following the N-body simulations and semi-analytical models (eg. Kravtsov et al. 2004; Zheng et al. 2005), we assume that the number of satellites inside a parent halo forms a Poisson distribution. Thus we have $\langle N_s(N_s - 1) \rangle = N_s^2$.

4.3 The two halo term

The correlation between satellite-satellite and satellite-central pairs located in different halos also modifies the 2-halo term. In this case the expression for scale dependent galaxy bias in Eq. (18) can be modified by adding in the contribution from satellite galaxies. Note that each halo of mass M has $N_s(L_{th}, M, z)$ satellite galaxies, brighter than L_{th} . Thus the number density of satellite galaxies associated with a halo in any mass interval M and $M + dM$ is $n(M, z)N_s(L_{th}, M, z)dM$. These satellites are residing in a parent halo with a large scale bias $b(M, z)$. Therefore, the average galaxy bias obtained by adding the contributions of both the central and satellite galaxies is,

$$b_g(k, z, L_{th}) = \frac{1}{n_g^T(L_{th}, z)} \int dM n(M, z) b(M, z) \left[f_{cen}(L_{th}, M, z) + \langle N_s | L_{th}, M, z \rangle \right] u(k, M, z). \quad (28)$$

If halos do not host any satellite galaxies, ie $\langle N_s | L_{th}, M, z \rangle = 0$, this expression reduces back to Eq. (18). We can now compute the two halo term by substituting Eq. (28) into Eq. (5) and using Eq. (12).

4.4 The total luminosity function

One may wonder if the additional satellite galaxies inside a halo can modify the luminosity function. In this section we compute the contribution to galaxy luminosity function from visible satellite galaxies. The total luminosity function

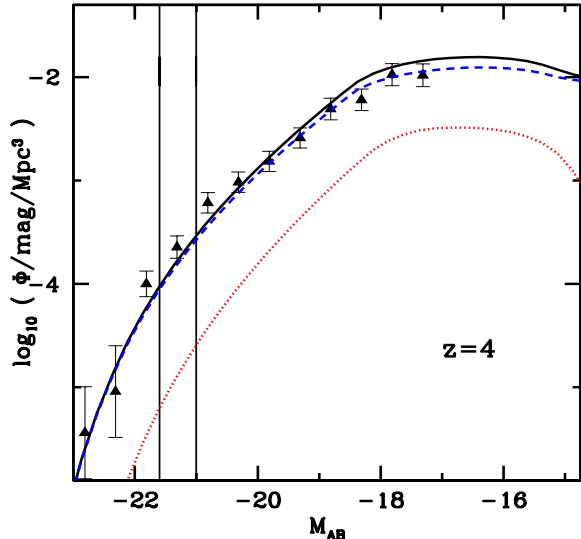


Figure 8. The best fit luminosity function of LBGs at $z = 4$ (solid-black) including the contribution from satellite galaxies. Also shown is the individual luminosity functions due to central (dashed-blue) as well as satellite (dotted-red) galaxies. The vertical (solid-black) lines are drawn at absolute magnitudes -21.0 and -21.6 .

of LBGs at any redshift can be written as,

$$\Phi(M_{AB}, z) = \Phi_{cen}(M_{AB}, z) + \Phi_{sat}(M_{AB}, z). \quad (29)$$

In section 2 we computed the luminosity function due to central galaxies. The contribution to luminosity function due to satellite galaxies can be written as,

$$\Phi_{sat}(M_{AB}, z)dM_{AB} = \int dM \frac{\rho_m}{M} \varphi(M, M_{AB}, z) n(M, z). \quad (30)$$

In Fig. 8 we have plotted the luminosity functions of both central and satellite galaxies separately at $z = 4$. It is clear that the number density of satellite galaxies (red dotted curve) at any given M_{AB} is roughly an order of magnitude less compared to that of central galaxies (blue dashed curve) at any luminosity bin. Thus the contribution to total luminosity function (solid black curve) due to satellite galaxies is negligible at any given luminosity. However, these satellites can still contribute to the small scale clustering. As discussed earlier, the typical mass M_P of parent halos hosting satellite galaxies is roughly 2 times the average halo mass M_{av} of a detectable LBG itself. As the luminosity roughly scales with halo mass, the central galaxy in the parent halo could then be about 2 times (or about 0.60 magnitudes) brighter. From Fig. 8, we can see that satellite galaxies with absolute magnitude say -21 , in a parent halo of mass M_P , will be about a third as abundant as the central galaxies, with absolute magnitude -21.6 , in them. Such pairs which will then occur in every third parent halo of mass M_P (hosting a detectable galaxy) will contribute significantly to the small angular scale clustering.

5 COMPARISONS WITH OBSERVATIONS

5.1 The total correlation functions

The total two point correlation function of galaxies at any scale is the sum of the contributions from one halo and two halo terms (as given in Eq. (14)). This can be converted to the angular correlation functions using Eq. (13). We again adopted the same fiducial model with $\kappa = 1.0$ and three different M_{agn} values, $0.8 \times 10^{12} M_\odot$, $1.5 \times 10^{12} M_\odot$, and $3.0 \times 10^{12} M_\odot$ at redshifts 3, 4 and 5 respectively (κ and M_{agn} are described in Table 1). The cosmological parameters are kept to their fiducial value. We also use $\Delta t_0 = 1.6 t_{dyn}$, $1.5 t_{dyn}$ and $1.4 t_{dyn}$ at $z = 3, 4$ and 5 respectively for all the models, but test the sensitivity of the results to this choice. This free parameter will correspond to different redshift intervals Δz_0 at $z = 3, 4$ and 5 . Various parameters of our fiducial model are tabulated in Table. 4.

The total angular correlation functions computed using our prescription for three redshifts and three threshold magnitudes are overplotted on the observed data in Fig. 9. In this figure the blue solid curves are our predictions of total galaxy angular correlation functions for the fiducial model. The dotted and dashed curves are for $\Delta t_0 = 1.0 t_{dyn}$ and $2 t_{dyn}$ respectively. We see that adopting the fiducial Δt_0 values quoted above provides a better fit to the data at small angular scales, for all redshifts and magnitudes. A smaller (larger) Δt_0 leads generically to an excess (deficit) of small angular scale clustering. The black dash-dotted lines show the contribution to correlation function due to central galaxies alone (computed in Section 3 and given in Fig. 4). The satellite galaxies contribute negligibly to clustering at large angular scales, as suggested earlier in Section 3. The remaining contribution, which dominates especially at small angular scales ($\theta < 10''$), is mainly due to the one halo term. It is also clear that the one halo term does not affect clustering on large angular scales ($\theta > 10''$). Note that the one halo and two halo contributions are distinctly seen in the observed data for $z = 3$ and $z = 4$ as predicted by our models. But these distinct contributions are not so clearly seen in the $z = 5$ data.

From the figure it is clear that our simple physical model gives a reasonable fit to the observed angular correlation functions at large ($\theta > 80''$) and small ($\theta < 10''$) angular scales. This is true at all magnitude thresholds and at all redshifts. Moreover at $z = 3$ the the predicted angular correlation functions fits the observed data reasonably well at all angular scales (including the range $10'' < \theta < 80''$), for magnitude thresholds 25.0 and 25.5. However, for the most luminous galaxies at $z = 3$ (with $m < 24.5$), and for redshifts 4 and 5, there is a discrepancy in the intermediate scales between the theoretically predicted correlation function and observed data points.

In order to explore these issues further, we now consider the LBG clustering measurements at $z = 4$ by Ouchi et al. (2005), which extends to much fainter galaxies with $m \leq 27.5$. We show in Fig. 10 our model predictions of correlation functions at $z = 4$ along with observed data (red squares) given by Ouchi et al. (2005). In this figure the predicted angular correlation functions with $\Delta t_0 = 1.5 t_{dyn}$, that fits the Hildebrandt et al. (2009) data, is shown in blue solid lines. The dotted and dashed blue curves are obtained respectively by adopting Δt_0 to be $1.0 t_{dyn}$ and $1.25 t_{dyn}$.

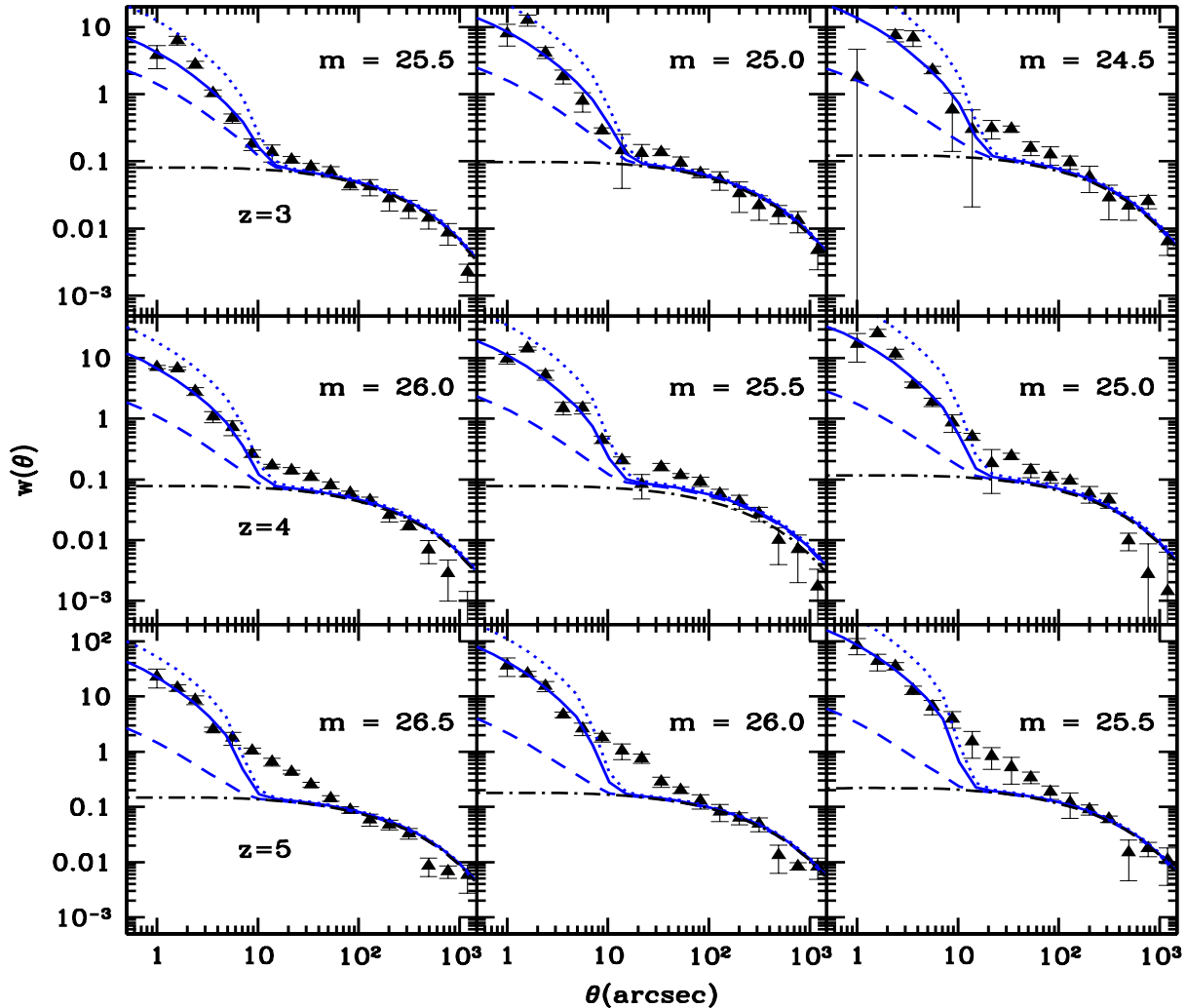


Figure 9. The angular correlation function of LBGs, taking into account the one halo and the two halo terms, at redshifts 3, 4 and 5 for various limiting magnitudes. Each row corresponds to a particular redshift, which is labelled in the first panel of that row. In each row there are three panels showing the clustering predictions for galaxies with three threshold magnitudes, that are also labelled in the respective panels. Our fiducial model predictions of galaxy angular correlation functions with $\Delta t_0 = 1.6t_{dyn}, 1.5t_{dyn}$ and $1.4t_{dyn}$ at $z = 3, 4$ and 5 respectively are shown in blue solid lines. The dotted and dashed curves are for $\Delta t_0 = t_{dyn}$ and $2t_{dyn}$ respectively. The black dash-dotted lines show the correlation functions computed without satellite contribution (see Fig. 4). The data points and error bars shown by solid black triangles are from Hildebrandt et al. (2009).

Note that here we have used the appropriate redshift distribution of galaxies ($N(z)$ in Eq.13) as in Ouchi et al. (2005).

It is clear from Fig. 10, that for the fainter galaxy sample ($m \geq 26.5$), our physical model predicts a better fit to observed $w(\theta)$ even at the intermediate scales ($10'' < \theta < 80''$). Note that this was also the case for the faintest LBGs at $z = 3$ (see Fig. 9). The typical mass of dark matter halo hosting a galaxy increases with its luminosity. For example, we find that the minimum mass of the dark matter halos that can host a galaxy with $m < 27.5$ is $4.8 \times 10^{10} M_\odot$ compared to $5.7 \times 10^{11} M_\odot$ for a galaxy with $m < 25.0$. The higher order (quasi-linear) corrections to dark matter halos bias (Cooray & Sheth 2002) is expected to increase with the mass of the halos (Scannapieco & Barkana 2002; Iliev et al.

2003). This then suggests that the discrepancy at intermediate scales seen in Fig. 9 could be due to missing quasi-linear (higher order) bias in our models.

One can also see from Fig. 10 that, for fainter galaxies, a smaller value of Δt_0 gives a better fit to the small scale clustering ($\theta < 10''$). For example, for LBGs with $m = 25.0 - 26.0$, the fiducial value $\Delta t_0 = 1.35t_{dyn}$ gives a good fit to the observed small scale clustering. However, for fainter LBGs with $m = 27.5$, one requires a smaller $\Delta t_0 \sim 1.0t_{dyn}$ to obtain a good fit on small angular scales. Since the typical masses of fainter galaxies are smaller than that of brighter galaxies, this suggests that the parameter Δt_0 could be a function of the masses of the parent and satellite galaxies. Such a mass dependence could be an issue to probe further

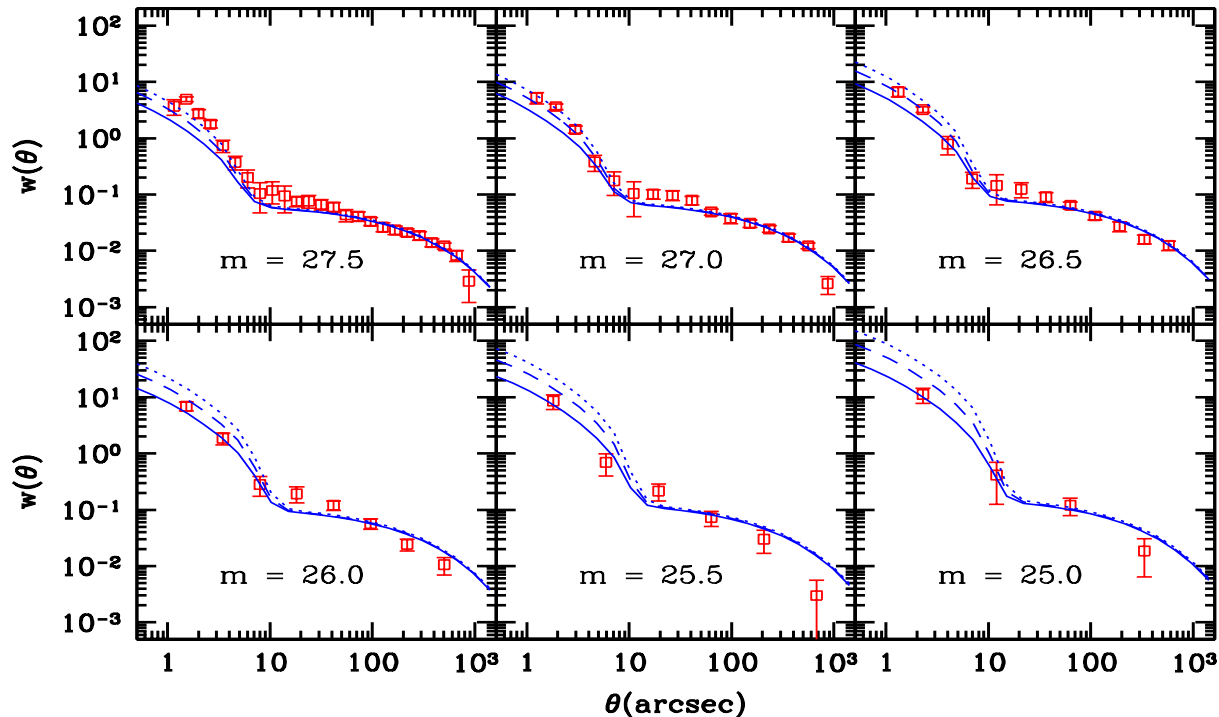


Figure 10. The angular correlation function of LBGs, taking into account the one halo and the two halo terms, at redshift 4 for various limiting magnitudes. Our fiducial model predictions of galaxy angular correlation functions with $\Delta t_0 = 1.5 t_{dyn}$ is shown in blue solid line. The dotted and dashed blue curves are obtained respectively by adopting Δt_0 to be $1.0 t_{dyn}$ and $1.25 t_{dyn}$. The data points and error bars shown by red squares are from Ouchi et al. (2005).

in the future when the small angular scale clustering data becomes more extensive. It could for example reflect the fact that the SFR of satellites is dependent on the properties of the parent halos.

Note that our model predictions of the large angular scale clustering is almost free of parameters, once we fix the cosmology and f_*/η from fitting the LFs of LBGs. We have given in Table 4, the reduced chisquare χ^2_ν obtained by comparing the predicted angular correlation function in the range $80'' < \theta < 600''$ with the observed data given by both Hildebrandt et al. (2009) ($\chi^2_\nu(H)$) and Ouchi et al. (2005) ($\chi^2_\nu(O)$). One can also see from the values of χ^2_ν given in the table, that our model predictions reasonably fits all the data, except for the $m = 26.5$ sample at $z = 5$ (where there is one discrepant data point).

Note that the discrepancy that we have found between model predictions for the brightest LBGs and the observed clustering data at intermediate scales, is also present in some of the previous works (see Fig. 9 and 10 of Lee et al. (2009) and Fig. 5 and 6. of Hamana et al. (2004)). As we have argued above this is likely to be due to quasi-linear corrections to the bias for the brightest LBGs. In addition to these higher order corrections to the bias, the missing clustering power at intermediate scales could also be due to (i) uncertainties related to distribution of satellite galaxies that is assumed to follow the NFW density profile of dark matter halos, (ii) the non-linear corrections to dark matter power spectrum (Mo & White 1996); although we find this does

not raise the predicted clustering to the observed values. We thus discuss possibility (i) further below. Nevertheless, it is quite remarkable that the predictions from our simple physical model fit the observed clustering over a wide range of magnitudes, scales and for the full range of $z = 3 - 5$.

5.2 Sensitivity to the halo density profile

The discrepancy noted above, between the observed and our model predicted $w(\theta)$ at intermediate angular scales, could be due to one halo correlations of galaxies extending beyond the virial diameter of NFW density profile. Physically this means that subhalos (and satellite galaxies they host) can reside outside the virial diameter of the parent halo. If this is true, data suggest that, this effect is stronger for $z \geq 5$.

To explore this possibility we assumed that halos follow a new density profile which is of the same form as the NFW profile, but with a larger virial radius $\bar{r}_{vir} = s_{vir} r_{vir}$. We keep the the concentration parameter and the mass of the parent halo the same as before. We took the fiducial values of $s_{vir} = 1.5$ and $s_{vir} = 2.0$ at redshifts 4 and 5 respectively (see Table 4). Adopting $s_{vir} > 1$ can increase the clustering at intermediate scales but will reduce the amplitude at small scales. This can be compensated by adopting a smaller Δt_0 . In Fig. 11 we have shown the effect of extending the one halo term beyond the virial diameter of the parent halo. The value of Δt_0 is also reduced to $1.4 t_{dyn}$ and $1.3 t_{dyn}$ respectively at redshifts 4 and 5 to obtain a better

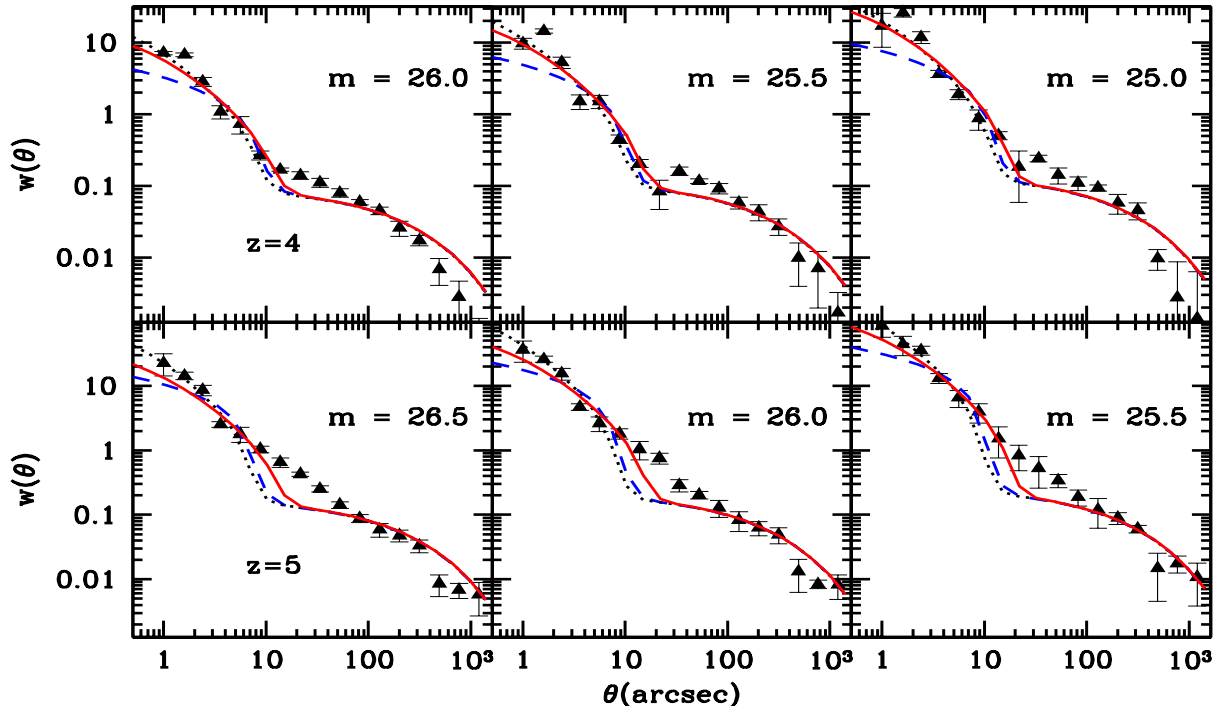


Figure 11. The effect of concentration parameter and s_{vir} on the clustering. Our fiducial model is shown in black dotted curve. The dashed blue curve is for a model where one uses concentration parameter given by Bullock et al. (2001). The solid red line shows our model predictions, that show the effect of extending the one halo term beyond the virial radius of the parent halo. In these cases, for simplicity, we multiplied the virial radius by factor s_{vir} . For $z=5$ we have used $s_{vir} = 2$ and for $z=4$ we have used $s_{vir} = 1.5$. Note that our fiducial model corresponds to $s_{vir} \sim 1$. The data points and error bars are from Hildebrandt et al. (2009). We used the fiducial cosmology parameters in this figure. All the astrophysical parameters the same as in Fig. 9.

fit at the smallest angular scales. The dotted black curve is for $s_{vir} = 1.0$ (fiducial model). The curves obtained after extending the one halo term beyond the virial diameter of dark matter halos are shown in solid red lines. One can clearly see that these new curves provide a better fit to the observed clustering in small angular scales ($\theta < 20''$). It is also clear from the figure that a change in the form of distribution of satellite galaxies inside the halos alone will not explain the discrepancy seen at $20'' \leq \theta \leq 80''$.

We have also considered the prescription for the concentration parameter given by Bullock et al. (2001), which is used by earlier works high redshift clustering (Hamana et al. 2006). The dashed blue curves in Fig. 11 show the corresponding results at $z = 4$ and 5 . One can clearly see that adopting the concentration parameter given by Bullock et al. (2001) underpredicts the clustering at $\theta \leq 3''$

5.3 Dependence on astrophysical and cosmological parameters

In Section 3.1, we found that the large angular scale correlation functions (with $80'' < \theta < 1300''$) were fairly insensitive to changes in the assumed astrophysical and cosmological parameters, provided these models still fit the observed LF. We now ask if this is true also for small angular scales below $\theta < 10''$ where our fiducial models can reasonably fit

the observed data. On small angular scales, the correlation functions can in principle be a function of astrophysical parameters as these change the total number of central and satellite galaxies satisfying the given luminosity criteria.

In Fig. 12, we show the effect of varying κ (which determines the duration of star formation activity in a halo) on small scale clustering. The blue solid curves are for our fiducial model with $\kappa = 1.0$. The blue dotted and dashed curves are for κ values 0.7 and 1.3 respectively. All other parameters except for f_*/η have been kept the same, and f_*/η is varied such that the predicted LF still fits the observed LF data reasonably well. One can clearly see that clustering predictions especially for $\kappa = 0.7$ do not fit the correlation functions on small angular scales. Therefore we conclude that small scale clustering of LBGs at high redshifts can give useful information about κ and thus the duration star formation in a halo. We find that $\kappa \sim 1$ or the star formation duration of order t_{dyn} is favored by the small scale clustering data.

We also varied M_{agn} , which determines the AGN feedback, around the fiducial value at each redshift, ensuring that the predicted LFs still reasonably fits the and observed data. We find that even the small scale angular correlation functions are fairly insensitive to these changes. For example when we varied M_{agn} at redshift 4 from $1.2 \times 10^{12} M_\odot$ to $1.8 \times 10^{12} M_\odot$, the clustering predictions change at all

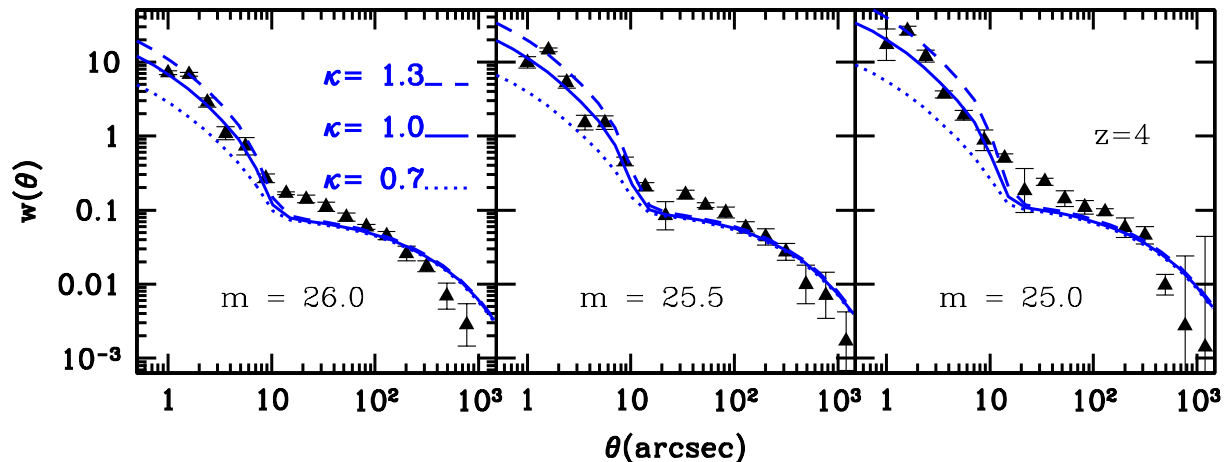


Figure 12. The change in angular correlation function with κ around its fiducial value at $z = 4$. The blue solid curve is the fiducial model prediction with $\kappa = 1.0$. The dotted and dashed curves are for $\kappa = 0.7$ and 1.3 respectively.

Table 4. A summary of the fiducial parameters used in various models at $z = 4, 5$ and 6 . The quantity κ that determines the duration of star formation in our models is fixed to be 1. For models where we extend one halo term beyond the virial diameter of a halo, we changed Δt_0 slightly from fiducial value.

z	m	$\frac{M_{agn}}{10^{12} M_{\odot}}$	$\frac{\Delta t_0}{t_{dyn}}$	s_{vir}	$\chi^2_{\nu}(H)$	$\chi^2_{\nu}(O)$
	24.5	0.8	1.6	1.0	0.8	
3	25.0	0.8	1.6	1.0	0.4	
	25.5	0.8	1.6	1.0	0.6	
	25.0	1.5	1.5	1.0	3.6	1.6
4	25.5	1.5	1.5	1.0	1.4	0.8
	26.0	1.5	1.5	1.0	3.8	2.9
	26.5	1.5	1.5	1.0		1.3
	27.0	1.5	1.5	1.0		0.2
	27.5	1.5	1.5	1.0		0.3
		1.5	1.4	1.5		
	25.5	3.0	1.4	1.0	1.3	
5	26.0	3.0	1.4	1.0	1.3	
	26.5	3.0	1.4	1.0	5.7	
		3.0	1.3	2.0		

scales by about -7% to 5% from the fiducial model. We also found that the situation is similar for all magnitudes and other redshifts.

We have also considered the effect of varying a whole suite of cosmological parameters within their 2σ limits determined by WMAP7 year data. Again we ensure that the predicted LFs best fits the observed data, by varying f_*/η . We find that the small angular scale clustering is very insensitive to changes in all the cosmological parameters except σ_8 ; where at most a $\pm 20\%$ change results when σ_8 is varied between its 2σ limits given by WMAP 7 year data.

6 DISCUSSION AND CONCLUSIONS

We have presented here a physically motivated semi-analytical model of galaxies to understand the clustering of high redshift Lyman break galaxies, where the model parameters are constrained by the observed high z luminosity function. For this purpose we use and expand upon the standard halo model. Galaxies are assumed to be formed inside dark matter halos. Their luminosity is determined by a physical model of star formation, which is a function of the mass and age of the hosting halo.

We began by assuming that each halo can host at most one visible galaxy. On fitting the observed LF, we determine the relationship between the luminosity of a galaxy and the mass of its host halo. This allows us to calculate the large scale bias for LBGs satisfying any luminosity threshold. This bias is then folded in with the dark matter power spectrum to predict the two point spatial correlation function of these LBGs and hence the angular correlation function $w(\theta)$. For our fiducial model, we find that the predicted $w(\theta)$ compares very well with the observed data of both Hildebrandt et al. (2009) and Ouchi et al. (2005) at $\theta > 80''$, for the whole range of redshifts $z = 3 - 5$ and limiting luminosities (magnitudes) (see Figs. 4, 9, 10 and Table 4).

The predicted large scale galaxy bias b_g agrees well with that observationally determined by Hildebrandt et al. (2009) (see Table 2). At a given z the bias increases with increasing luminosity, while for a given L_{th} it increases with z . However, we find a smaller spread in b_g as a function of L_{th} at any given z compared to that of Hildebrandt et al. (2009). Remarkably, we find that the predicted large scale clustering of LBGs is fairly insensitive to the assumed astrophysical or cosmological parameters, provided we simultaneously fit the observed LF. This may point to an important internal consistency of our physical model; that if we fix the mass to light ratio correctly by using the LFs of LBGs, then the standard LCDM model correctly predicts the amplitude of their large scale clustering.

We then extended our approach by incorporating the Halo occupation distribution, which provides the distribu-

tion of galaxies inside dark matter halos. This is separated into the central, f_{cen} , and satellite, N_s , contributions. Often the HOD is modelled in a parametrized form. Instead we have adopted a more physical approach. We use our prescription for computing the LF to estimate f_{cen} . The conditional mass function and our star formation model are used to calculate the mean number and luminosity of satellite galaxies in a parent halo. An additional parameter, Δt_0 , is introduced in calculating N_s (see Table 1). If parent halo collapses at a time t_p , a subhalo can host a detectable galaxy only if it collapses at an earlier epoch, $t_s < t_p - \Delta t_0$. In order to explain the small angular scale clustering, one requires Δt_0 of order t_{dyn} , the dynamical time scale of the parent halo. A much smaller (or larger) Δt_0 leads generically to an excess (deficit) of small angular scale clustering.

The calculated forms of $f_{cen}(M, L_{th}, z)$ and $N_s(M, L_{th}, z)$ compare reasonably with that assumed in parametrized models of Hamana et al. (2006) and the simulations of Conroy et al. (2006). The average value of f_{cen} is typically 0.4. Thus, on the average, 40% of the halos above a minimum mass M_{min} (which itself depends on the luminosity threshold), at any given redshift, can host detectable central galaxies. Further the average value of N_s is about 0.02 – 0.04, or about 5 – 10% of the halos with detectable central galaxies, also will have a detectable satellite. Indeed it is such pairs which contribute to the small angular scale clustering. At $z = 4$ and for apparent magnitude thresholds in the range 25-26, the average mass of halos contributing to the observed clustering, M_{av} , ranges from $10^{12}M_\odot - 3.9 \times 10^{11}M_\odot$. At $z = 5$ these masses are smaller by a factor ~ 1.4 , while at $z = 3$ these masses are larger by a similar factor. At any given redshift and magnitude threshold, the typical mass M_P of parent halos hosting detectable satellite galaxies, are about 2 times larger than M_{av} .

Having obtained the HOD, we can calculate both the one halo and two halo contributions to the total correlation function of LBGs. Our simple physical model gives a reasonable fit to the observed clustering of LBGs at all angular scales for the faintest LBGs with $m \geq 25$ at $z = 3$ and for $m \geq 26.5$ at $z = 4$. At $z = 5$, and for the most luminous galaxies at $z = 3, 4$, the predicted $w(\theta)$ again fits the observed data well at both large ($\theta > 80''$) and small ($\theta < 10''$) angular scales. The clustering at small angular scales as mentioned above, is likely to be dominated by pairs of LBGs rather than rich clusters, as the number of detectable galaxies hosted by most collapsed halos is typically less than 2.

The small angular scale clustering is also not very sensitive to changes of several cosmological and astrophysical parameters from their fiducial values, as long as we simultaneously fit the observed LF. However, the amplitude of $w(\theta)$ on small angular scales is very sensitive to the value of κ , which determines the duration of star formation activity in a halo. The present data are consistent with $\kappa \sim 1$ or a star formation duration of the order of the dynamical time scale t_{dyn} of the dark matter halo.

We find that the following broad physical picture of LBGs consistently accounts for their observed LF and clustering. First the average mass of the halos hosting the brightest central LBGs at $z = 3 - 5$, with $-21 < M_{AB} < -20$, is around $3 \times 10^{11}M_\odot$ to $1.5 \times 10^{12}M_\odot$. Halos which host

detectable satellites and contribute dominantly to the small angular clustering are more massive by a factor of 2 or so. Typically fainter LBGs or those at higher z are hosted by smaller mass halos. In these galaxies about 50% of the stars are formed over a timescale of 300 – 500 Myr for $z = 5 - 3$, by converting $\sim 3 - 8\%$ of the baryons to stars. Our physical model for the HOD suggests that approximately 40% of the halos above a minimum mass M_{min} , can host detectable central galaxies. This is comparable to the duty cycle values preferred by Lee et al. (2009, 2012). Further, about 5 – 10% of these halos are likely to also host a detectable satellite. These satellites form over a dynamical timescale or so prior to the formation of the parent halo. The small angular scale clustering is mainly due to central-satellite pairs. The average fraction of halos which can host a central LBG can be compared to the duty cycle invoked in the literature. Finally, a preliminary study suggests that the star formation model that we have invoked is also consistent with observation of the SFR- M_* relation, and the stellar mass function.

The theoretically predicted $w(\theta)$ at intermediate angular scales is smaller than that observed, for the brightest LBGs at $z = 3, 4$ and at $z = 5$. We explored in detail whether this excess can be due to a more extended satellite galaxy distribution. This only partly accounts for the discrepancy. We also find that the non-linear corrections to dark matter power spectrum does not raise the predicted clustering at the intermediate scales to the observed values. Note that the typical mass of dark matter halo hosting a galaxy increases with its luminosity. Also the higher order (quasi-linear) corrections to the dark matter halo bias is expected to be larger for higher mass and higher redshift halos, which are rarer. Therefore we suspect that the higher order quasi-linear corrections to galaxy bias could be playing a role in explaining the excess intermediate scale clustering, a possibility which we hope to explore in the future. Nevertheless, it is noteworthy that the predictions from our simple physical model, employing only a few free parameters, can fit the observed clustering data over a wide range of scales, redshifts and limiting luminosities.

ACKNOWLEDGMENTS

We thank Hendrik Hildebrandt, Masami Ouchi and Nobunari Kashikawa for providing the observed data of angular correlation functions. CJ thanks Aseem Paranjpye for many discussions while writing the code to incorporate the halo model. CJ also acknowledges support from CSIR. KS acknowledges partial support from NSF grant PHY - 0903797 while visiting University of Rochester and Eric Blackman at Rochester for warm hospitality. SS acknowledges support from University of Kwazulu-Natal, South Africa. We thank an anonymous referee for very detailed and useful comments which helped us to improve our paper.

REFERENCES

- Adelberger K. L., Steidel C. C., Giavalisco M., Dickinson M., Pettini M., Kellogg M., 1998, ApJ, 505, 18
- Adelberger K. L., Steidel C. C., Pettini M., Shapley A. E., Reddy N. A., Erb D. K., 2005, ApJ, 619, 697

- Benson A. J., Bower R. G., Frenk C. S., Lacey C. G., Baugh C. M., Cole S., 2003, *ApJ*, 599, 38
- Benson A. J., Lacey C. G., Baugh C. M., Cole S., Frenk C. S., 2002, *MNRAS*, 333, 156
- Berlind A. A., Weinberg D. H., 2002, *ApJ*, 575, 587
- Berlind A. A. et al., 2003, *ApJ*, 593, 1
- Berrier J. C., Bullock J. S., Barton E. J., Guenther H. D., Zentner A. R., Wechsler R. H., 2006, *ApJ*, 652, 56
- Best P. N., Kaiser C. R., Heckman T. M., Kauffmann G., 2006, *MNRAS*, 368, L67
- Bielby R. M. et al., 2011, *MNRAS*, 414, 2
- Bouwens R. J., Illingworth G. D., Franx M., Ford H., 2007, *ApJ*, 670, 928
- Bouwens R. J., Illingworth G. D., Franx M., Ford H., 2008, *ApJ*, 686, 230
- Bouwens R. J. et al., 2012, *ApJ*, 754, 83
- Bower R. G., Benson A. J., Malbon R., Helly J. C., Frenk C. S., Baugh C. M., Cole S., Lacey C. G., 2006, *MNRAS*, 370, 645
- Bromm V., Loeb A., 2002, *ApJ*, 575, 111
- Bullock J. S., Kolatt T. S., Sigad Y., Somerville R. S., Kravtsov A. V., Klypin A. A., Primack J. R., Dekel A., 2001, *MNRAS*, 321, 559
- Bullock J. S., Wechsler R. H., Somerville R. S., 2002a, *MNRAS*, 329, 246
- Bullock J. S., Wechsler R. H., Somerville R. S., 2002b, *MNRAS*, 329, 246
- Chiu W. A., Ostriker J. P., 2000, *ApJ*, 534, 507
- Choudhury T. R., Srianand R., 2002, *MNRAS*, 336, L27
- Conroy C., Wechsler R. H., Kravtsov A. V., 2006, *ApJ*, 647, 201
- Cooray A., Ouchi M., 2006, *MNRAS*, 369, 1869
- Cooray A., Sheth R., 2002, *Phys. Rep.*, 372, 1
- Dijkstra M., Haiman Z., Rees M. J., Weinberg D. H., 2004, *ApJ*, 601, 666
- Giavalisco M., Dickinson M., 2001, *ApJ*, 550, 177
- González V., Bouwens R. J., Labbé I., Illingworth G., Oesch P., Franx M., Magee D., 2012, *ApJ*, 755, 148
- González V., Labbé I., Bouwens R. J., Illingworth G., Franx M., Kriek M., 2011, *ApJ*, 735, L34
- González V., Labbé I., Bouwens R. J., Illingworth G., Franx M., Kriek M., Brammer G. B., 2010, *ApJ*, 713, 115
- Hamana T., Ouchi M., Shimasaku K., Kayo I., Suto Y., 2004, *MNRAS*, 347, 813
- Hamana T., Yamada T., Ouchi M., Iwata I., Kodama T., 2006, *MNRAS*, 369, 1929
- Hildebrandt H., Pielorz J., Erben T., van Waerbeke L., Simon P., Capak P., 2009, *A&A*, 498, 725
- Iliev I. T., Scannapieco E., Martel H., Shapiro P. R., 2003, *MNRAS*, 341, 81
- Jing Y. P., Mo H. J., Boerner G., 1998, *ApJ*, 494, 1
- Jose C., Samui S., Subramanian K., Srianand R., 2011, *Phys. Rev. D*, 83, 123518
- Kashikawa N. et al., 2006, *ApJ*, 637, 631
- Khochfar S., Silk J., Windhorst R. A., Ryan, Jr. R. E., 2007, *ApJ*, 668, L115
- Kravtsov A. V., Berlind A. A., Wechsler R. H., Klypin A. A., Gottlöber S., Allgood B., Primack J. R., 2004, *ApJ*, 609, 35
- Labbé I. et al., 2010, *ApJ*, 716, L103
- Larson D. et al., 2011, *ApJS*, 192, 16
- Lee K.-S. et al., 2012, *ApJ*, 752, 66
- Lee K.-S., Giavalisco M., Conroy C., Wechsler R. H., Ferguson H. C., Somerville R. S., Dickinson M. E., Urry C. M., 2009, *ApJ*, 695, 368
- Lee K.-S., Giavalisco M., Gnedin O. Y., Somerville R. S., Ferguson H. C., Dickinson M., Ouchi M., 2006, *ApJ*, 642, 63
- Leitherer C. et al., 1999, *ApJS*, 123, 3
- Madau P., Ferguson H. C., Dickinson M. E., Giavalisco M., Steidel C. C., Fruchter A., 1996, *MNRAS*, 283, 1388
- Mo H. J., White S. D. M., 1996, *MNRAS*, 282, 347
- More S., van den Bosch F. C., Cacciato M., Mo H. J., Yang X., Li R., 2009, *MNRAS*, 392, 801
- Navarro J. F., Frenk C. S., White S. D. M., 1997, *ApJ*, 490, 493
- Oke J. B., Gunn J. E., 1983, *ApJ*, 266, 713
- Ouchi M. et al., 2005, *ApJ*, 635, L117
- Ouchi M. et al., 2004, *ApJ*, 611, 685
- Peebles P. J. E., 1980, *The large-scale structure of the universe*
- Porciani C., Giavalisco M., 2002, *ApJ*, 565, 24
- Prada F., Klypin A. A., Cuesta A. J., Betancort-Rijo J. E., Primack J., 2012, *MNRAS*, 3206
- Reddy N. A., Pettini M., Steidel C. C., Shapley A. E., Erb D. K., Law D. R., 2012, *ApJ*, 754, 25
- Reddy N. A., Steidel C. C., Pettini M., Adelberger K. L., Shapley A. E., Erb D. K., Dickinson M., 2008, *ApJS*, 175, 48
- Samui S., Srianand R., Subramanian K., 2007, *MNRAS*, 377, 285
- Samui S., Srianand R., Subramanian K., 2009a, *MNRAS*, 398, 2061
- Samui S., Subramanian K., Srianand R., 2008, *MNRAS*, 385, 783
- Samui S., Subramanian K., Srianand R., 2009b, *New A*, 14, 591
- Samui S., Subramanian K., Srianand R., 2010, *MNRAS*, 402, 2778
- Savoy J., Sawicki M., Thompson D., Sato T., 2011, *ApJ*, 737, 92
- Scannapieco E., Barkana R., 2002, *ApJ*, 571, 585
- Scoccimarro R., Sheth R. K., Hui L., Jain B., 2001, *ApJ*, 546, 20
- Seljak U., 2000, *MNRAS*, 318, 203
- Sheth R. K., Hui L., Diaferio A., Scoccimarro R., 2001, *MNRAS*, 325, 1288
- Sheth R. K., Tormen G., 1999, *MNRAS*, 308, 119
- Skibba R. A., Sheth R. K., 2009, *MNRAS*, 392, 1080
- Somerville R. S., Primack J. R., 1999, *MNRAS*, 310, 1087
- Somerville R. S., Primack J. R., Faber S. M., 2001, *MNRAS*, 320, 504
- Springel V. et al., 2005, *Nature*, 435, 629
- Stark D. P., Ellis R. S., Bunker A., Bundy K., Targett T., Benson A., Lacy M., 2009, *ApJ*, 697, 1493
- Stark D. P., Loeb A., Ellis R. S., 2007, *ApJ*, 668, 627
- Steidel C. C., Adelberger K. L., Dickinson M., Giavalisco M., Pettini M., Kellogg M., 1998, *ApJ*, 492, 428
- Steidel C. C., Giavalisco M., Dickinson M., Adelberger K. L., 1996, *AJ*, 112, 352
- Tinker J. L., Weinberg D. H., Zheng Z., Zehavi I., 2005, *ApJ*, 631, 41
- van den Bosch F. C., Yang X., Mo H. J., 2003, *MNRAS*, 340, 771

- van der Burg R. F. J., Hildebrandt H., Erben T., 2010, A&A, 523, A74
 Wilkins S. M., Gonzalez-Perez V., Lacey C. G., Baugh C. M., 2012, MNRAS, 424, 1522
 Yang X., Mo H. J., van den Bosch F. C., 2003, MNRAS, 339, 1057
 Zehavi I. et al., 2004, ApJ, 608, 16
 Zehavi I. et al., 2011, ApJ, 736, 59
 Zehavi I. et al., 2005, ApJ, 630, 1
 Zheng Z. et al., 2005, ApJ, 633, 791
 Zheng Z., Zehavi I., Eisenstein D. J., Weinberg D. H., Jing Y. P., 2009, ApJ, 707, 554

different values of σ_8 , say σ_8^A and σ_8^B . The ratio between two point correlation functions of both models on large scales will be

$$\frac{\xi_{2h}^A}{\xi_{2h}^B} = \left(\frac{\sigma_8^B}{\sigma_8^A}\right)^2 \left(\frac{M_{av}^A}{M_{av}^B}\right)^{\frac{2(3+n_{eff})}{3}} \quad (\text{A6})$$

For galaxies we have $n_{eff} \sim -2$. Hence the ratio between galaxy two point correlation functions of models A and B is given by

$$\frac{\xi_{2h}^A}{\xi_{2h}^B} = \left(\frac{\sigma_8^B}{\sigma_8^A}\right)^2 \left(\frac{M_{av}^A}{M_{av}^B}\right)^{\frac{2}{3}} \quad (\text{A7})$$

APPENDIX A: CLUSTERING DEPENDENCE ON σ_8

For any mass scale M , the variance of smoothed density contrast $\sigma^2(M) \propto \sigma_8^2 k_M^3 P(K_M) \sim \sigma_8^2 k_M^{3+n_{eff}}$. Here n_{eff} is the effective spectral index, which is ~ -2 on galactic scales and -1 on cluster scales. We also have $k_M^{-1} \sim M^{1/3}$. Thus we get

$$\sigma^2(M) \propto \sigma_8^2 M^{-\frac{(3+n_{eff})}{3}}. \quad (\text{A1})$$

For high redshifts $\nu(M, z) = (\delta_c(z)/\sigma(M))^2 \gg 1$. Hence using Eq. 7 we get the halo bias, $b(M, z) \propto \nu(M, z) \propto 1/\sigma^2(M)$. Using A1 in this, the scaling of halo bias at high redshifts can be written as

$$b(M, z) \propto \frac{M^{\frac{3+n_{eff}}{3}}}{\sigma_8^2}. \quad (\text{A2})$$

We know that on large scales galaxy bias $b_g(k, z, L_{th})$ given by Eq. (10) is a constant (or k independent). To get the scaling behavior of this galaxy bias we assume that in Eq. (10) the major contribution to galaxy bias comes from masses at and around M_{av} . In this limit $b_g(k, z, L_{th}) \sim b(k, M_{av})$. The quantity M_{av} is the average mass of the halo that can host a galaxy of luminosity L_{th} (See Fig. 3). It is clear that M_{av} depends on astrophysical and cosmological parameters. Also, as discussed in Section 3, on very large scales galaxy bias is scale independent. Thus using Eq. (A2) we get

$$b_g(z, L_{th}) \propto \frac{M_{av}^{\frac{3+n_{eff}}{3}}}{\sigma_8^2}. \quad (\text{A3})$$

The large scale (small k) dark matter power spectrum $P_{lin}(k)$ always scale as square of σ_8 . Hence using Eq. (11) and Eq. (A3) we get the following scaling law of galaxy power spectrum.

$$P_g^{2h}(k, L_{th}, z) = b_g^2(L_{th}, z) P_{lin}(k, z) \propto \frac{M_{av}^{\frac{2(3+n_{eff})}{3}}}{\sigma_8^2} \hat{F}(k, z) \quad (\text{A4})$$

where $P_{lin}(k, z) = \sigma_8^2 \hat{F}(k, z)$. The two point correlation functions on large scales also scale in this way. Thus under the above approximations

$$\xi_{2h}(L_{th}, R, z) \propto \frac{M_{av}^{\frac{2(3+n_{eff})}{3}}}{\sigma_8^2} F(R, z) \quad (\text{A5})$$

where $F(R, z)$ is the transformation of $\hat{F}(k, z)$ as given in Eq. (12) Suppose one assumes two models A and B with